Chapter 5. Fracture and Failure Analysis of GNP and Aligned Fe_3O_4-GNP Epoxy Nanocomposite

5.1. Introduction

This study presents an analysis of the mechanical properties of nanocomposites reinforced with GNP and aligned Fe_3O_4-GNP nanoparticles. The primary objective of this research is to investigate the influence of the alignment of Fe_3O_4-GNP on the mechanical properties of the nanocomposites. Furthermore, we have undertaken a comparative study between GNP and aligned Fe_3O_4-GNP reinforced nanocomposites. After conducting a comprehensive review of existing literature from various reputable sources, we have not come across any research articles that specifically focus on the following study. Based on our current understanding, we have not come across any published research on this specific topic

- Fabrication of properly dispersed GNP and Fe_3O_4-GNP reinforced nanocomposites, and aligned Fe_3O_4-GNP nanocomposites with optimised alignment parameters.
- An analysis comparing the tensile and compressive properties of nanocomposites reinforced with GNP and aligned Fe_3O_4-GNP
- The impact of Fe_3O_4-GNP alignment and the weight percentage of nanoparticles on fracture toughness mechanisms, including stress intensity factor (K_{IC}), strain energy release rate (G_{IC}), critical crack tip opening displacement ($CTOD_c$), and crack propagation
- Correlation between $CTOD_c$, wt% of nanoparticles, K_{IC} and G_{IC} for both GNP and aligned Fe_3O_4-GNP reinforced nanocomposites

- Analysing stereo zoom optical and atomic force microscopy (AFM) images of fractured surfaces in-depth to investigate the underlying mechanisms governing crack propagation and fracture toughness.
- A comprehensive analysis of fracture surface roughness parameters to investigate the $CTOD_c$, crack growth, and energy dissipation mechanisms.

5.2. Experimental

5.2.1. Basic Materials

As mentioned in section 4.2.1.

5.2.2. Preparation of GNP epoxy and aligned Fe_3O_4-GNP epoxy nanocomposites

As mentioned in section 4.2.3.

5.3. Mechanical properties

5.3.1. Tensile tests

Based on the ASTM D638 standard, tensile tests have been carried out on neat epoxy and its nanocomposites at room temperature (30 °C) to determine their maximum tensile load, maximum tensile extension, Young's modulus, yield strength, and toughness [196]. To prevent failure outside the gauge length due to significant stress concentrations, standard dumbbell-shaped Type I specimens have been cast in the silicon mould, as depicted in **Fig. 5.1**. The Instron 8801 UTM with a 30KN load cell was used for the tests, which were computer-controlled and performed with displacement control at a crosshead speed of 1 mm/min. The E-moduli have been computed using an Instron extensometer (2630-112) with a gauge length of 50 mm and a load in the 0.05-0.25% strain range[197]. At least five samples have been tested for each wt% loading.

5.3.2. Compression tests

In this section, a procedure for carrying out plane strain compression experiments has been presented, which has enabled the measurement of the compressive yield stress, along with an investigation of the response of cylindrical specimens measuring 10 mm x 10 mm, depicted in **Fig. 5.2**, when subjected to compression, as stipulated by Williams and Ford [198]. The specimens have been prepared and tested according to the ASTM D695 standard [199]. The Instron 8801 UTM with a 30KN load cell has been used for the tests, which have been computer-controlled and performed with displacement control at a crosshead speed of 1 mm/min. To achieve a smooth surface finish on the PSC samples, a LaboPol-21 polishing machine from Struers in Denmark has been used with progressively finer sandpaper grits, starting with 320 and ending with 4000. The contact surfaces have been lubricated with 'Molykote BR-2 Plus Grease' from Dow Corning, USA to reduce friction further. At least five samples have been tested for each wt% loading.

5.3.3. Compact tension (CT) test for fracture toughness

This section explains the procedure for conducting quasi-static fracture toughness tests using CT specimens that comply with ASTM D5045-99 and have dimensions of W =26 mm and B = 4.0 mm (**Fig. 5.3**). To achieve a smooth surface finish on the PSC samples, a LaboPol-21 polishing machine from Struers in Denmark has been used with progressively finer sandpaper grits, starting with 320 and ending with 4000. A sharp crack length (a) is created by tapping the notch tip with a fresh razor blade having a tip radius of 2 μm. To ensure accurate measurements of the plane strain K_{IC} or G_{IC} the specimens are subjected to post-curing to eliminate residual stresses caused by the tapping process, and the size criteria for the specimen are strictly followed [200].

$$B, a, (W - a) \geq 2.5\left(K_{IC}/\sigma_y\right)^2 \tag{5.1}$$

The Instron 8801 UTM with a 2KN load cell has been used for the tests, which have been computer-controlled and performed with displacement control at a crosshead speed of 1 mm/min. K_{IC}, which evaluates fracture toughness under plane strain, can be computed as follows[200]:

$$K_{IC} = \frac{P_{max} f(a/W)}{B\sqrt{W}} \tag{5.2}$$

Where, the thickness and breadth of a specimen are denoted by B and W, respectively and $f(a/W)$ has related to the sample's shape. The parameter P_{max} denotes the peak load recorded in the load-COD curve of CT specimens. For CT samples, f has been expressed as:

$$f(a/W) = f(\alpha) = \frac{2+\alpha}{(1-\alpha)^{3/2}}(0.886 + 4.64\alpha - 13.32\alpha^2 + 14.72\alpha^3 - 5.6\alpha^4) \tag{5.3}$$

To determine G_{IC}, two different methods were employed. The first method involved computing the net fracture area and the corresponding energy dissipation from the load-displacement curve of CT specimen. The second method used the values of E, ν, and K_{IC} derived via Eq. (5.3). The results obtained from both methods showed good agreement. Therefore, this study presents the values of G_{IC} obtained from Eq. (5.3). That is:

$$G_{IC} = \frac{(1-\nu^2)K_{IC}^2}{E} \tag{5.4}$$

where, ν, the Poisson's ratio has been taken 0.35[201], and Young's modulus (E) of each material system has been determined through a tensile test in accordance with ASTM D638, and more information is provided in next section.

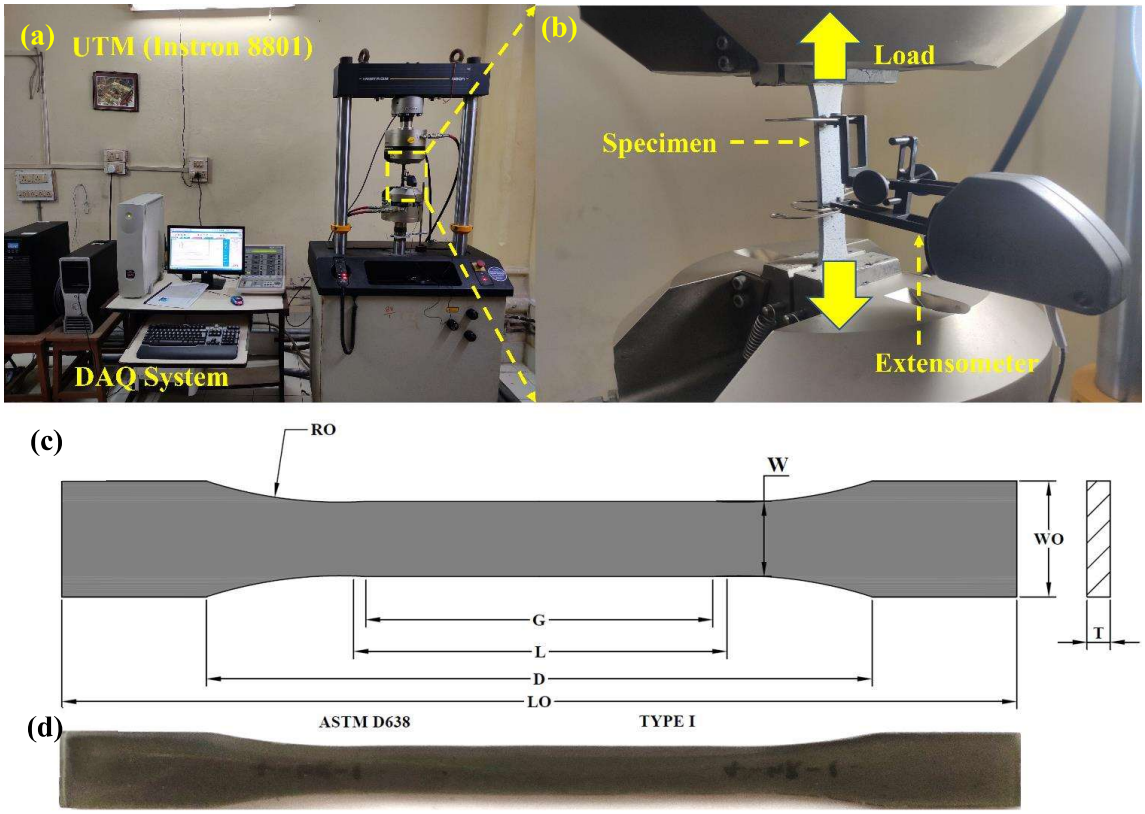

Fig. 5.1. Displays(a) and (b) the experimental set up of tensile testing, (c) ASTM for the tensile (d), and final nanocomposite specimen.

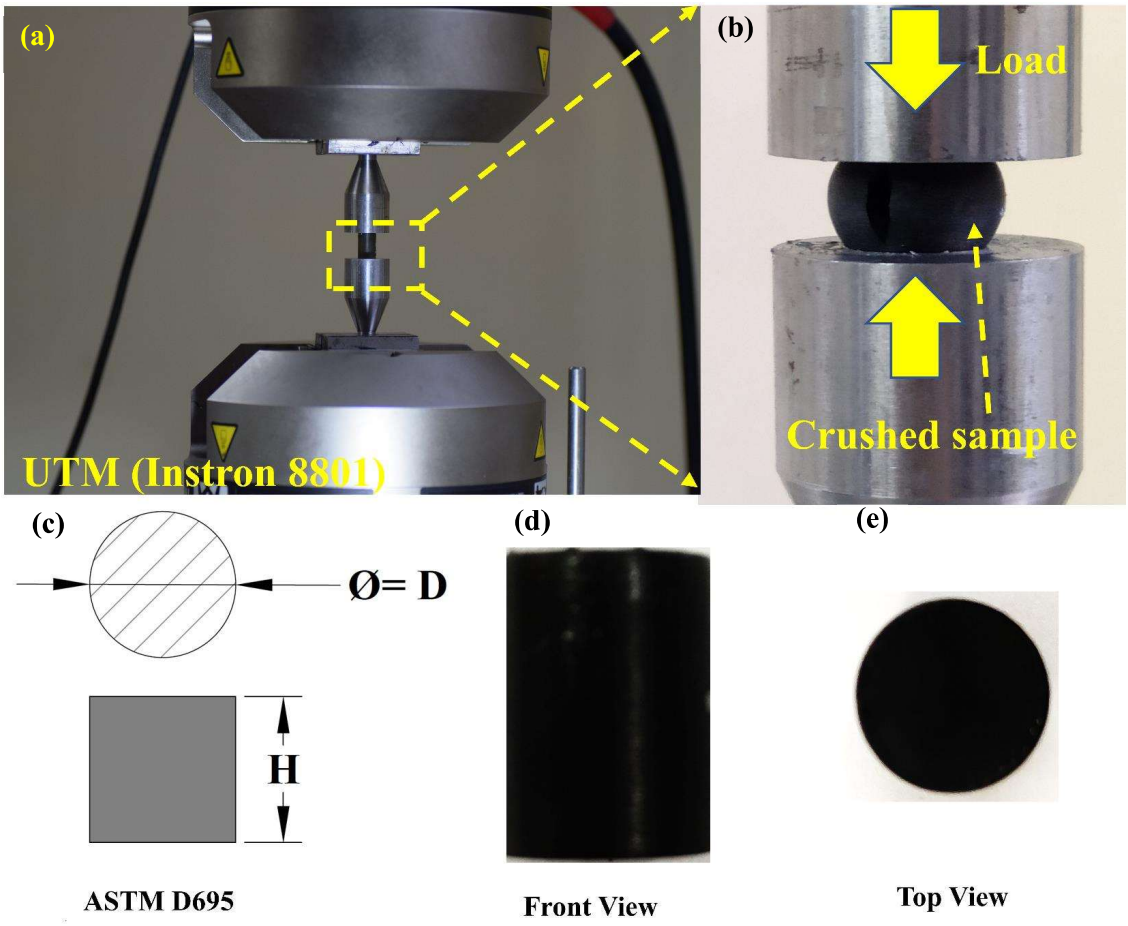

Fig. 5.2. Shows the experimental set up of compressive test (a) and (b), ASTM for the test (c), and final prepared compressive specimen (d) and (e).

5.3.4. *CTOD$_c$* measurement by clip gauges

CTOD$_c$ has long been recognised as a reliable indicator of fracture properties of brittle materials and has served as a valuable index to track crack growth in plastic fracture analysis. It is a widely accepted assessment of material toughness and fracture resistance, measured as the displacement required to initiate stable crack growth[202]. Its utility lies in the determination of critical crack size that leads to structural failure, with higher *CTOD$_c$* values signifying greater toughness. *CTOD$_c$* has found extensive applications in testing and designing structural components, developing new materials, and analysing fracture behaviour in different environments. Its ability to measure displacement close to the crack tip has enabled the direct

characterisation of crack-tip stress and deformation fields, as illustrated in (**Fig. 5.4**). Critical crack opening displacement(COD_c) has been computed using an Instron *COD* gauge (2670-116) having a gauge length of 10 mm and an output sensitivity of 2.5 mV/V +1% -3% at 20 °C[197]. After carefully measuring the CODc at the front face, the $CTOD_c$ was computed using a complex mathematical formula considering various factors. The resulting $CTOD_c$ value is crucial for determining the material's fracture toughness as[203]:

$$CTOD_C = \frac{\frac{X_0}{W} - \frac{a}{W}}{\frac{X_0}{W} + 0.25} COD_C \tag{5.5}$$

where $\frac{X_0}{W}$ is evaluated to find the position of the rotational axis.

$$\frac{X_0}{W} = -0.0995314 + 3.02437\left(\frac{a}{W}\right) - 7.95768\left(\frac{a}{W}\right)^2 + 13.546\left(\frac{a}{W}\right)^3 - 10.6274\left(\frac{a}{W}\right)^4 + 3.1133\left(\frac{a}{W}\right)^5 \tag{5.6}$$

5.3.5. Fracture surface analysis

We used a stereo zoom optical microscope to examine fractured surfaces to understand better the deformation and failure mechanisms induced by nanoparticles under loading. This lets us look at micrographs of the surface and make a qualitative assessment of the surface's texture and how cracks propagate across it. The stereo zoom optical microscope we used was a Model RSM 9, IS300, 3.0MP, purchased from Radical Scientific. We also employed an atomic force microscopy (AFM) examination with a scanning probe microscope (SPM) (NTEGRA Prima, NT-MDT Service & Logistics Ltd.) to determine the post-fracture surface roughness parameters of nanocomposites. Specifically, we scanned randomly chosen 10 μm x10 μm spots near the crack points and captured the scanned parts at a relatively high resolution using the tapping technique [204]. The AFM micrograph was further analysed using Gwyddion, which

is free, open-source software for visualising and analysing data from scanning probe microscopy techniques [205].

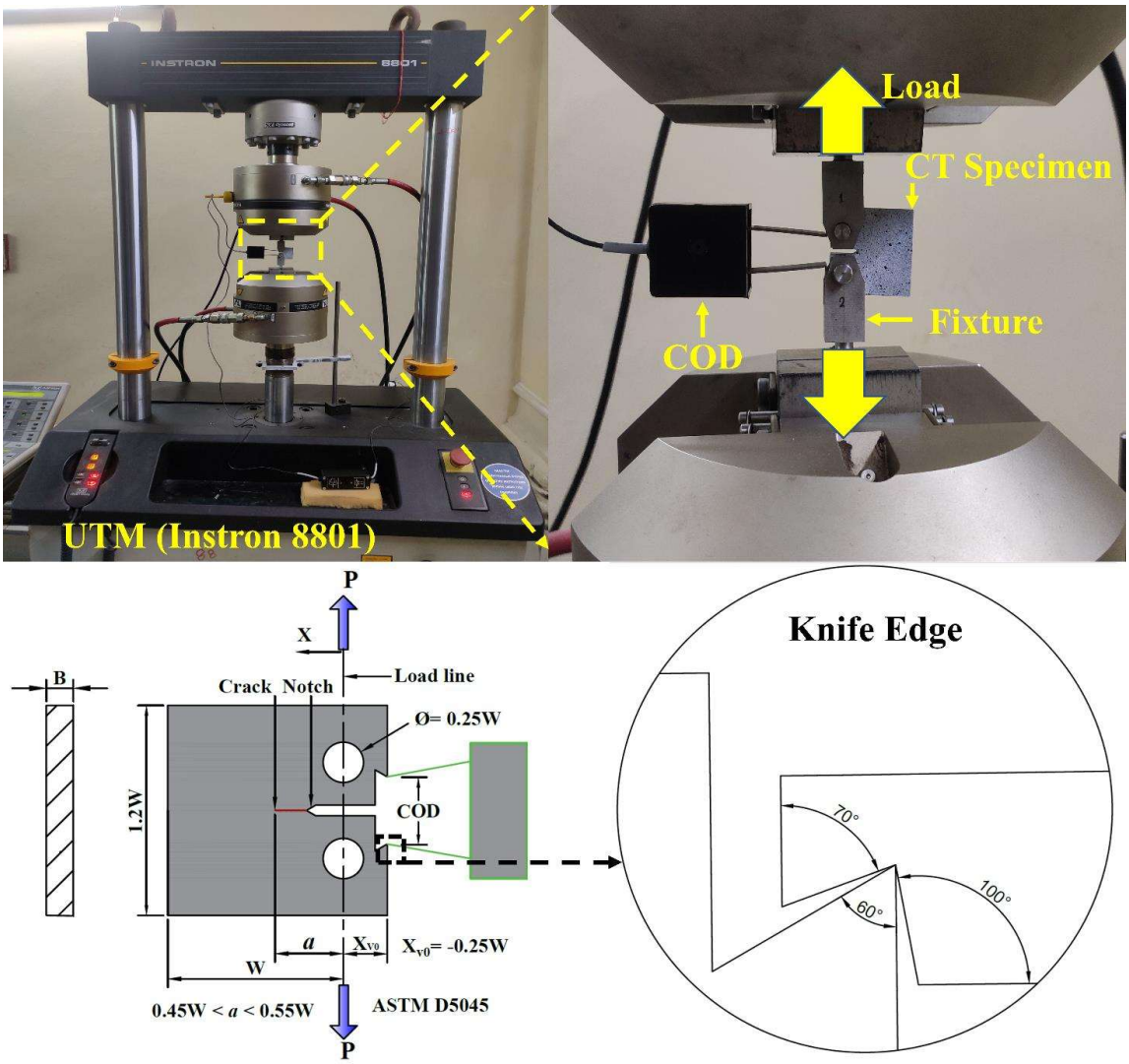

Fig. 5.3. Visualises the experimental set up, ASTM of fracture testing, and knife edge configuration at *COD* tips.

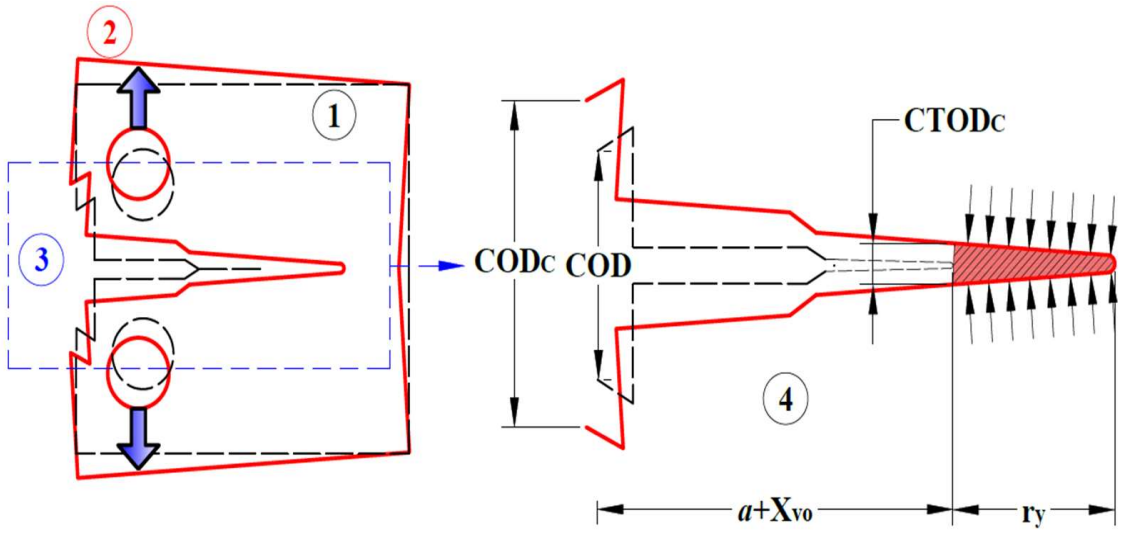

Part No.	Discription
1	Undeformed Specimen
2	Deformed Specimen
3	Zoom Section
4	Hypothetical Crack Under Load

Fig. 5.4. Demonstrates the hypothetical crack openning configuration and growth phenomena under the Mode-I loading.

5.4.Results

5.4.1. Tensile Properties

The reinforcement effect in nanocomposites refers to increased tensile properties when reinforced with nanoparticles such as GNP and aligned Fe_3O_4-GNP. It is influenced by parameters like load transfer, stress concentration, and defect distribution, affecting the mechanical properties of nanocomposites. The impact of nanoparticle concentration is evident from the engineering stress and strain curves for neat epoxy, GNP, and aligned Fe_3O_4-GNP at

different concentrations (**Fig. 5.5**). Comprehending the reinforcement effect is crucial in understanding the tensile properties of nanocomposites.

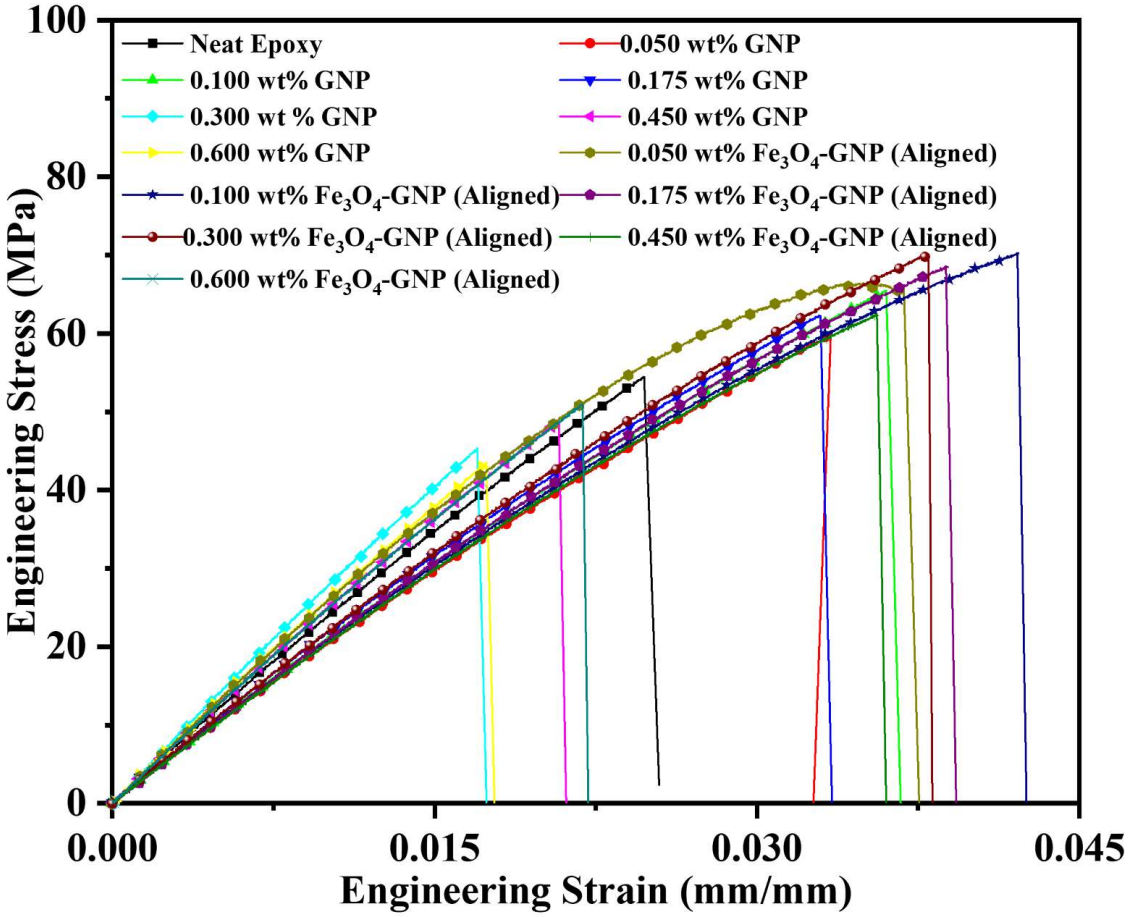

Fig. 5.5. Indicates the engineering stress and engineering strain behaviour of the nanocomposites under tensile loading at crosshead rates of 1 mm/min and ambient conditions (30 0C, humidity 50%).

5.4.1.1. Maximum tensile load

This section presents data on the maximum tensile load of random and aligned nanoparticles from **Fig. 5.6**. Initially, the maximum load increases to 0.100 wt%, but it decreases and falls below neat epoxy. The maximum load for aligned nanoparticles at 0.100 wt% is more significant than for random nanoparticles. The research shows that the maximum tensile load percentage achieved is 29% more than neat epoxy, but higher loading results in decreased maximum tensile load capacity [206]. The ultimate tensile load of random and aligned nanoparticles increases initially but eventually drops, with higher loading leading to decreased maximum tensile load capacity.

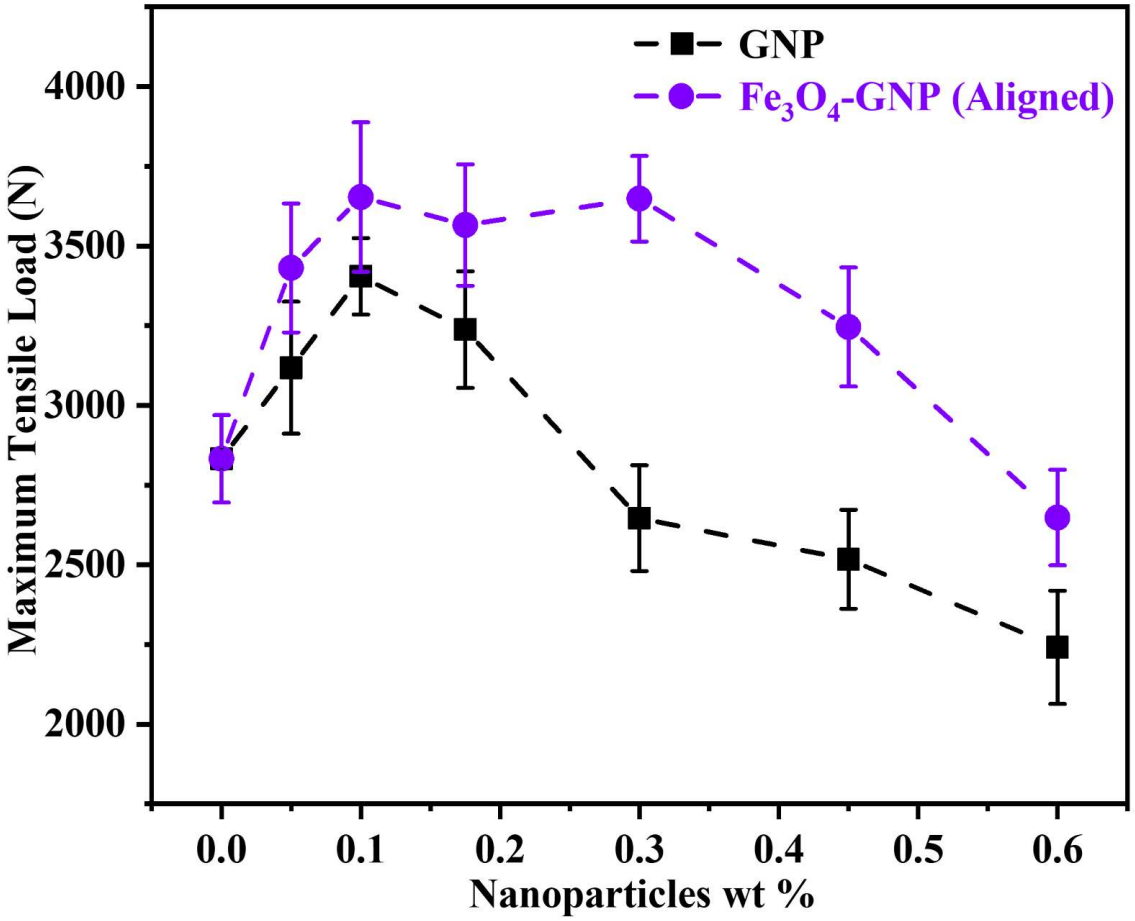

Fig. 5.6. Shows the maximum tensile load sustained by the nanocomposite under tensile loading with different nanoparticle weight percentages. The error bar represents the Standard Deviation of data.

5.4.1.2. Maximum tensile extension

Fig. 5.7 shows the ultimate extension of nanocomposites vs nanoparticle weight percentage. The maximum extension of nanocomposites increases with nanoparticle loading up to 0.100 wt% but decreases beyond that. Only four nanocomposites showed less extension than others, suggesting that ductility rises up to a specific limit. The study's results provide insight into nanocomposites' behaviour under tensile loading, indicating their properties can be improved by controlling nanoparticle loading within a specific range. Further research is needed to explore the reasons for the decrease in extension beyond 0.100 wt%.

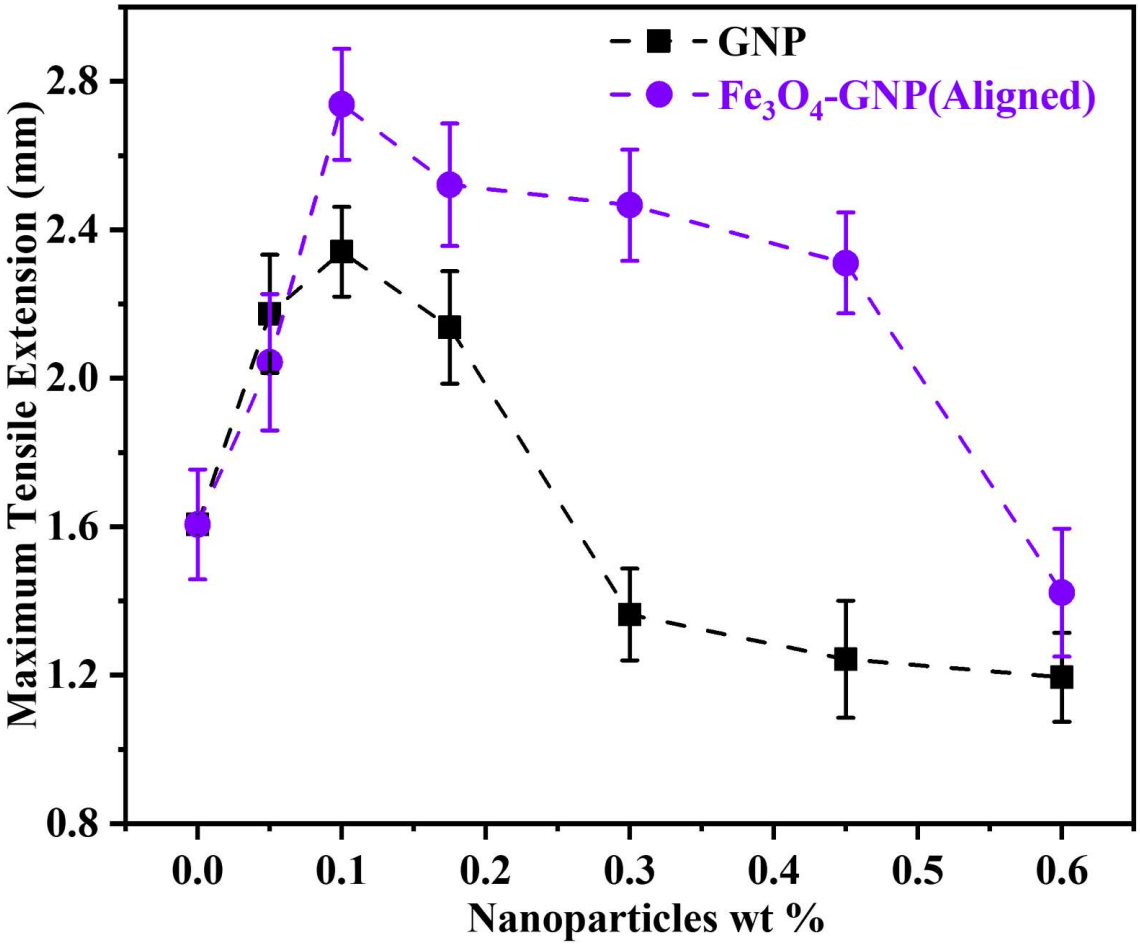

Fig. 5.7. Displays the maximum tensile extension sustained by the nanocomposite under tensile loading with different nanoparticle weight percentages. The error bar represents the Standard Deviation of data.

5.4.1.3. Young's modulus

The presented data in **Fig. 5.8** shows the tensile modulus measurement of the neat epoxy and the impact of adding nanoparticles on Young's modulus of the nanocomposite. The tensile modulus of neat epoxy is 3.7 ± 0.120 GPa, which improves by adding nanoparticles. The nanocomposite with aligned nanoparticles has a higher tensile modulus than the one with randomly oriented nanoparticles, with the highest reported value of 4.84 ± 0.11 GPa in the nanocomposites with aligned nanoparticles at 0.600 wt%. Such an improvement can offer better mechanical properties to the nanocomposite.

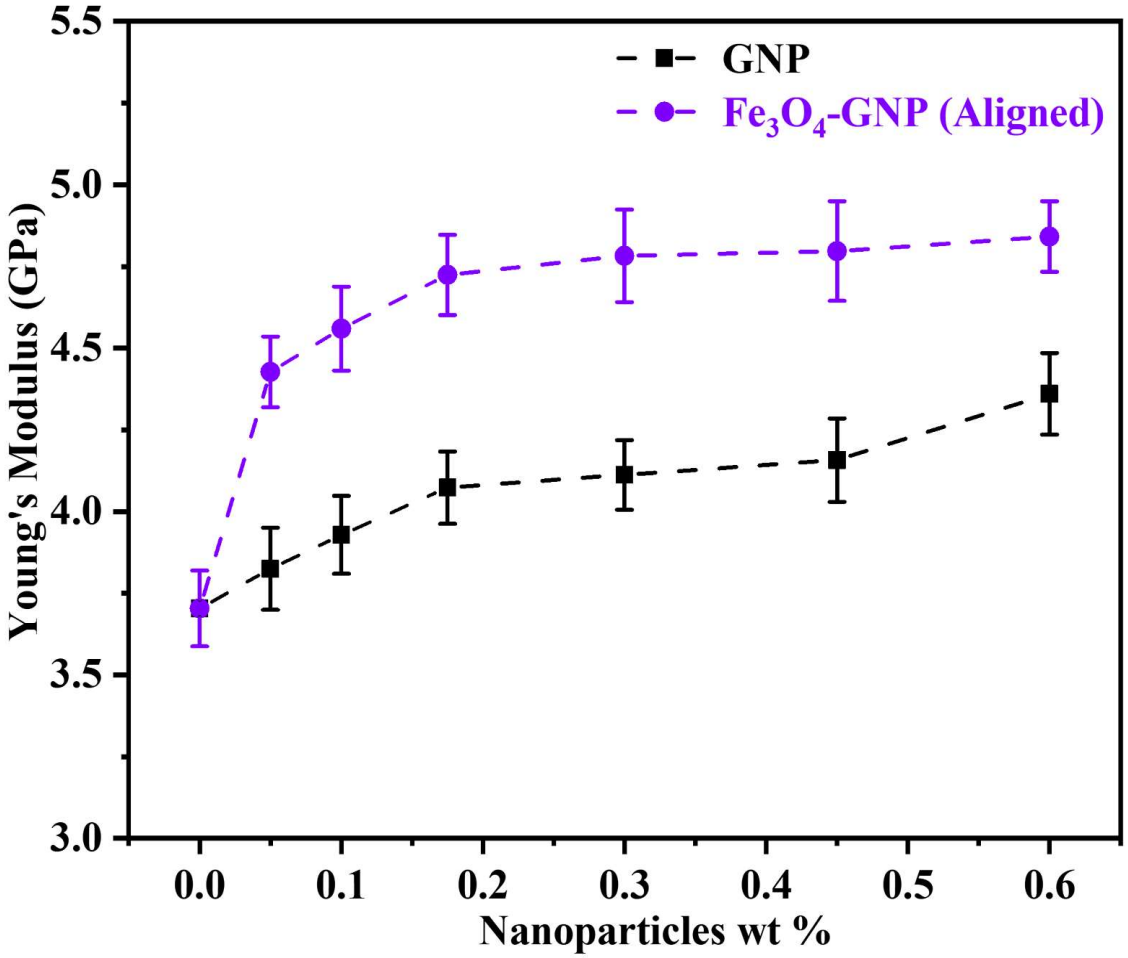

Fig. 5.8. Shows the Young's Modulus of the nanocomposite under tensile loading with different nanoparticle weight percentages. The error bar represents the Standard Deviation of data.

5.4.1.4. Yield strength

Based on **Fig. 5.9** analysis, the study investigated the Yield strength of GNP and aligned Fe_3O_4-GNP nanocomposites with varying nanoparticle loadings. Aligned Fe_3O_4-GNP nanocomposites showed higher Yield strength than those with GNP at the same nanoparticle loading. Specifically, the 0.100 wt% aligned Fe_3O_4-GNP nanocomposites exhibited the highest Yield strength of about 70.26 ± 4.56 MPa, 29.15% higher than pure epoxy. The protruding Fe_3O_4 nanoparticles on the surface of GNP nanoplatelets contributed to micro-crazing, which limited the propagation of cracks into larger ones in the polymer nanocomposites. Incorporating aligned

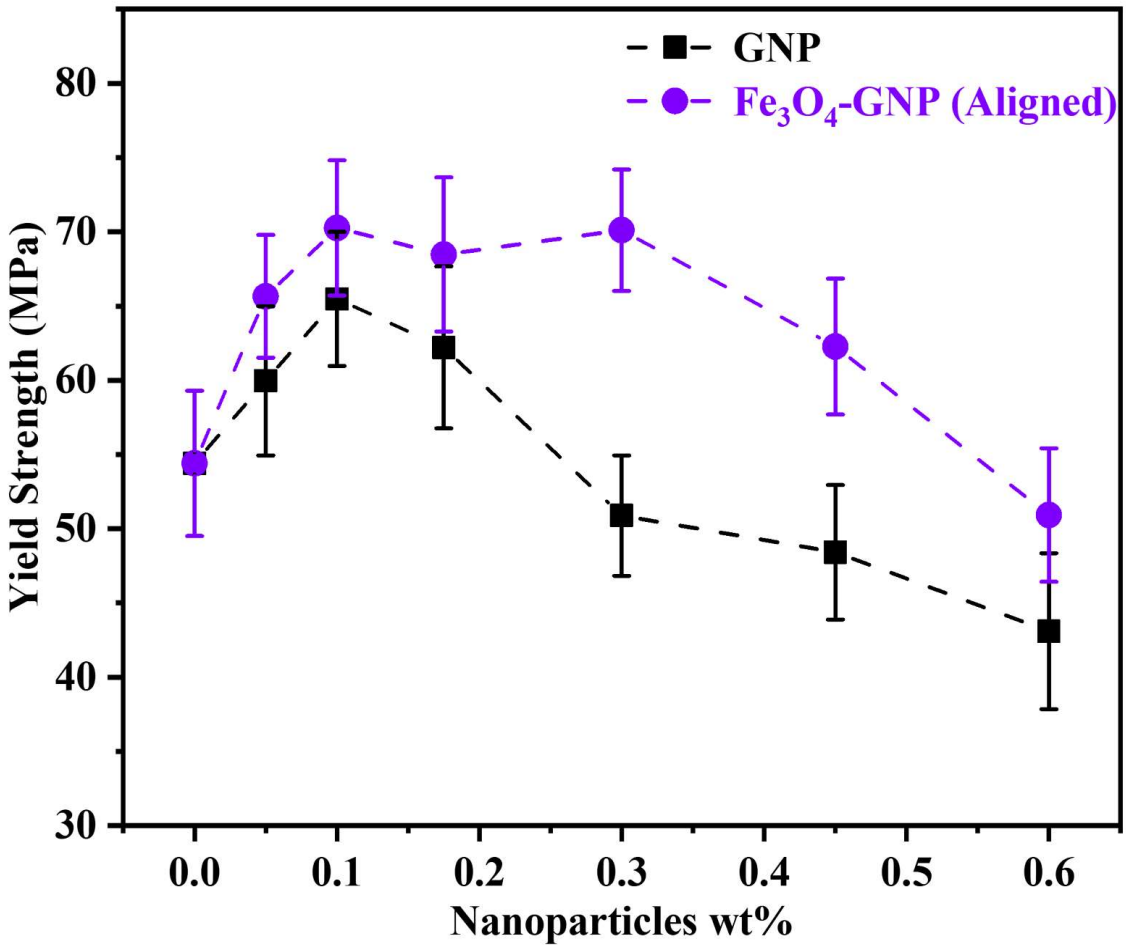

Fig. 5.9. Shows the Yield strength of the nanocomposite under tensile loading with different nanoparticle weight percentages. The error bar represents the Standard Deviation of data.

Fe_3O_4-GNP nanoparticles in the polymer matrix can significantly enhance the nanocomposites' mechanical properties.

5.4.1.5. Toughness

Toughness is a material's ability to absorb energy before rupturing without fracturing and differs from fracture toughness which resists loads in the presence of flaws (discussed in section 5.4.3). Nanocomposites reinforced with aligned Fe_3O_4-GNP and GNP exhibit increasing toughness as nanoparticle loading increases until a certain point, after which it decreases (**Fig. 5.10**). Aligned Fe_3O_4-GNP nanocomposites are tougher than GNP nanocomposites, with the highest toughness observed at 0.100 wt% loadings, 110.493% higher than pure epoxy. GNP nanocomposites have a toughness of 3.65 ± 0.365J, which is only 53.72% higher than pure epoxy. The lowest toughness is observed at 0.600 wt% loadings.

Loading GNP and aligned Fe_3O_4-GNP nanoparticles can enhance material properties such as maximum load, maximum extension, tensile strength, and yield strength up to 0.100wt%. Although the toughness initially increases with loading, it eventually decreases after reaching a certain point. Nanoparticle loading affects the toughness of nanocomposites, but it also improves other mechanical properties.

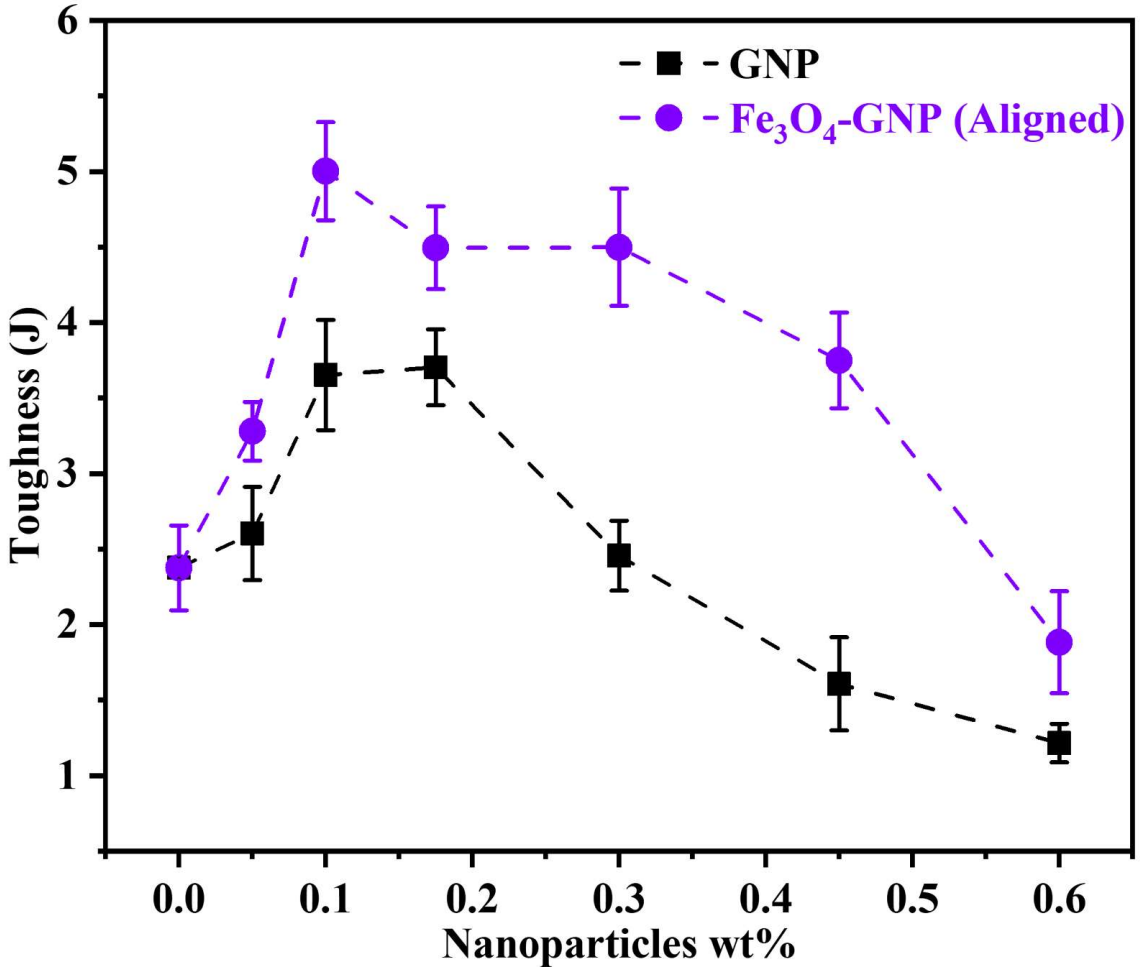

Fig. 5.10. Shows the toughness of the nanocomposite under tensile loading with different nanoparticle weight percentages. The error bar represents the Standard Deviation of data.

5.4.2. Compression Properties

The compressive stress-strain curves of neat epoxy, GNP, and aligned Fe_3O_4-GNP at varying weight percentages are shown in **Fig. 5.11**, indicating that the compressive behaviour of each nanocomposite changes with nanoparticle concentration. The compressive behaviour of nanocomposites is significantly affected by aligned nanoparticles, and comprehending this behaviour is crucial for developing structural materials with improved mechanical properties. This study highlights the potential applications of nanocomposites in the creation of novel structural materials.

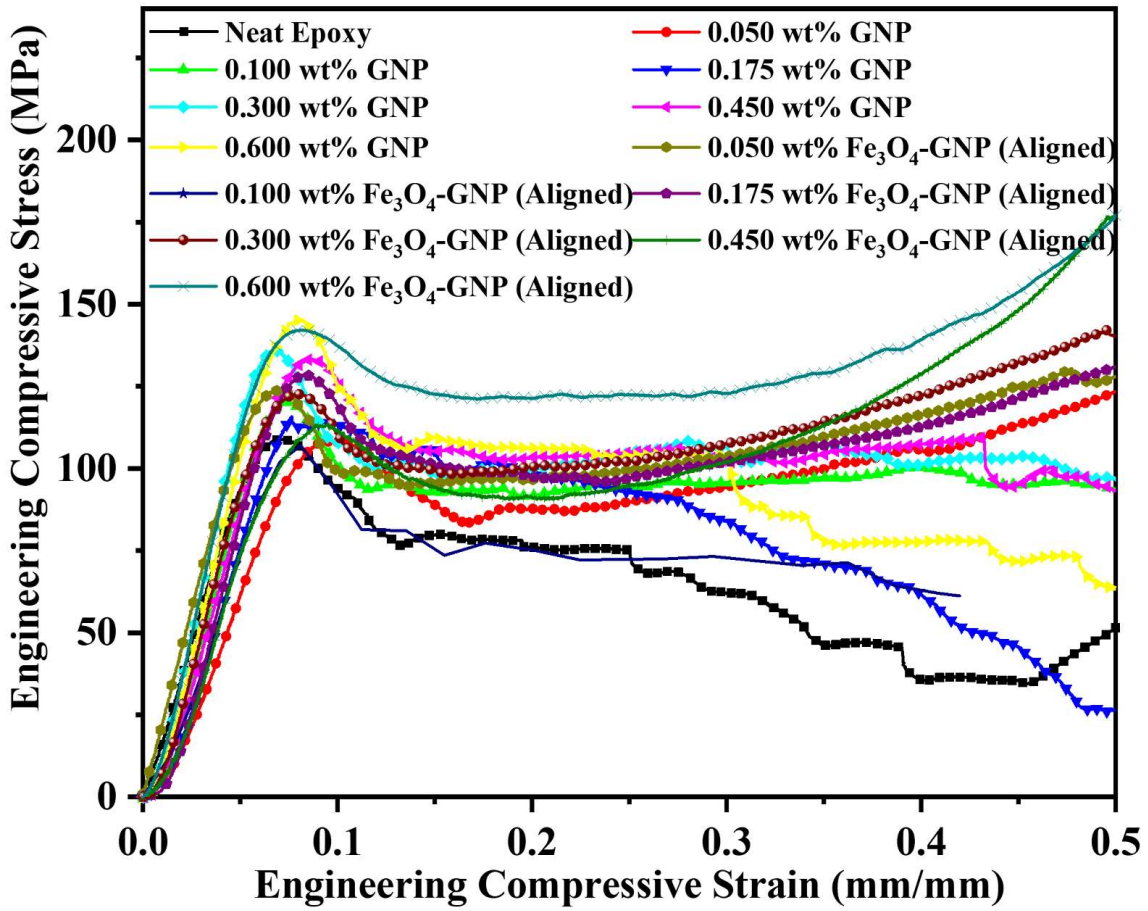

Fig. 5.11. Visualise the engineering compressive stress and engineering compressive strain behaviour of the nanocomposites under compressive loading at crosshead rates of 1 mm/min and ambient conditions (30 ^{0}C, humidity 50%)..

5.4.2.1. Compressive yield strength

This section discusses the impact of GNP and aligned Fe_3O_4-GNP nanoparticles on the compressive yield strength of a nanocomposite. Results presented in **Fig. 5.12** indicate that an increase in the loading weight percentage of both types of nanoparticles led to an increase in the compressive yield strength of the nanocomposite, with the aligned Fe_3O_4-GNP nanocomposite showing a higher growth. At 0.600 wt% loading weight percentage of both types of nanoparticles, the yield strength of the nanocomposite increased by 34.29% and 41.9% for GNP and aligned Fe_3O_4-GNP nanocomposites, respectively, compared to neat epoxy.

In conclusion, adding GNP and aligned Fe_3O_4-GNP nanoparticles significantly improved the compressive yield strength of the nanocomposite, making it an ideal candidate for high-performance structural materials in various fields where the strength and durability of materials are essential factors. Moreover, the consistently increasing trend observed for both types of nanoparticles suggests that the mechanical properties of the nanocomposite can be further enhanced by increasing the loading weight percentage of nanoparticles.

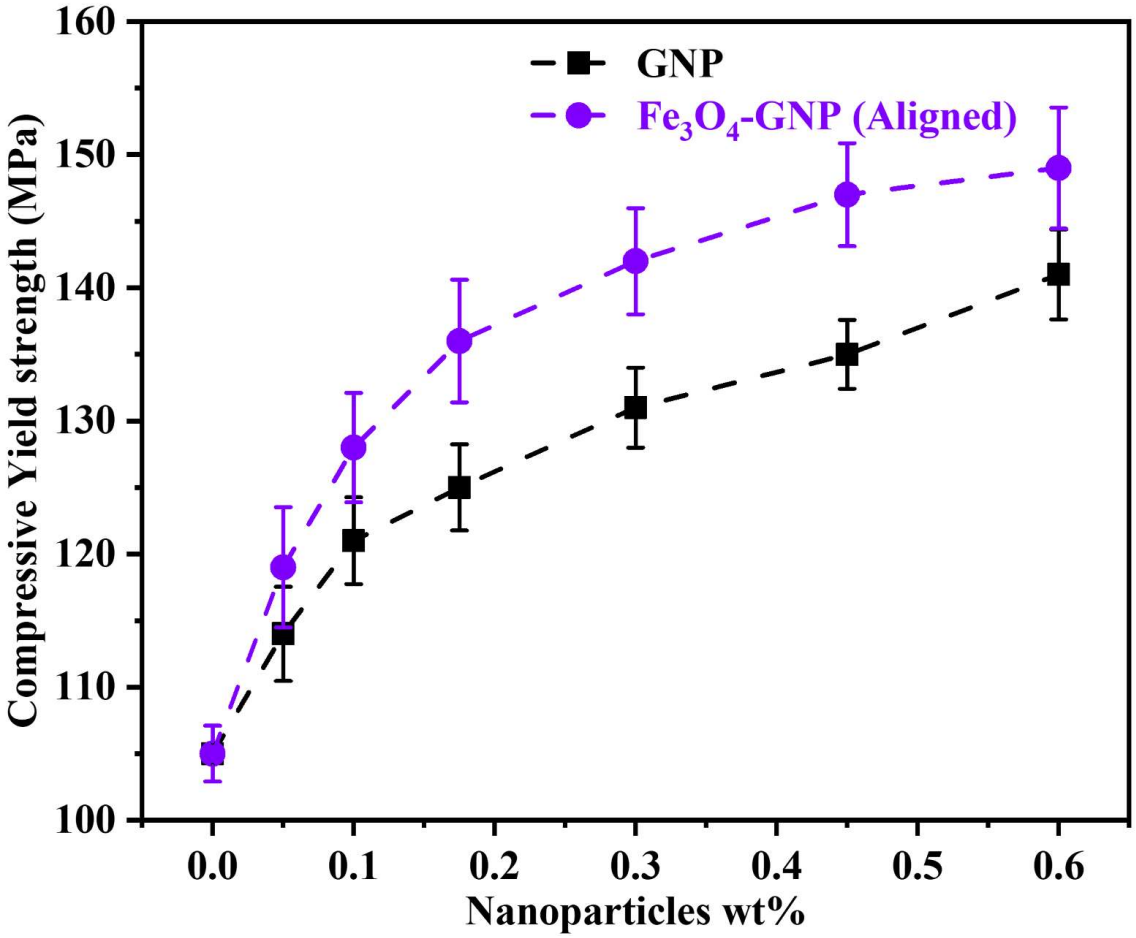

Fig. 5.12. Shows the compressive Yield strength of the nanocomposite under compressive loading with different nanoparticle weight percentages. The error bar represents the Standard Deviation of data.

5.4.2.2. Compressive modulus

Fig. 5.13 depicts a study on the compressive modulus of a nanocomposite with the addition of GNP and aligned Fe_3O_4-GNP nanoparticles. The research shows that adding nanoparticles increases the compressive modulus up to a certain concentration of 0.300 wt%. After that, the compressive modulus stays the same. Adding aligned Fe_3O_4-GNP nanoparticles resulted in a more significant improvement in the compressive modulus than GNP nanoparticles. The nanocomposite demonstrated greater improvement in incremental stiffness up to 0.100 wt% of nanoparticles loading, with the highest compressive modulus recorded at 0.600 wt% of both GNP and aligned Fe_3O_4-GNP nanoparticles, with values of 18.79% (2.21 ± 0.04 GPa) and 23.64% (2.28 GPa), respectively, concerning neat epoxy (1.86 ±0.060 GPa).

The study suggests that adding GNP and aligned Fe_3O_4-GNP nanoparticles can enhance the compressive modulus of the nanocomposite up to a specific concentration beyond which no further improvement is observed. The research also indicates that aligned Fe_3O_4-GNP nanoparticles may be more efficient in improving the compressive modulus than GNP nanoparticles.

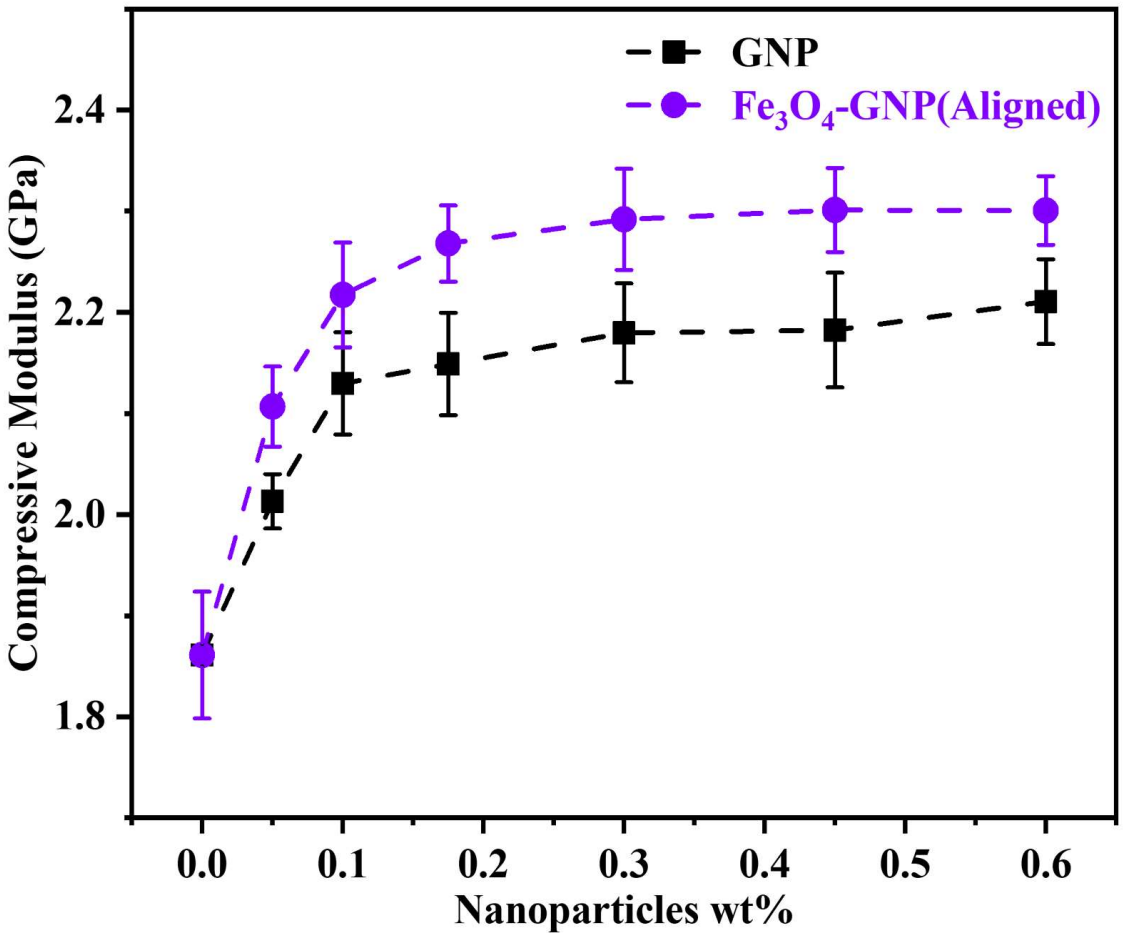

Fig. 5.13. Shows the compressive modulus of the nanocomposite under compressive loading with different nanoparticle weight percentages. The error bar represents the Standard Deviation of data.

5.4.3. Fracture toughness and fracture energy

The study investigated the impact of nanoparticles on the fracture toughness of neat epoxy and nanocomposites. Incorporating nanoparticles increased modulus and fracture toughness, with alignment being the primary factor. Loading the nanoparticles improved load-COD and capacity (**Fig.** 5.14). Nanoparticles can enhance fracture toughness in materials with design applications .

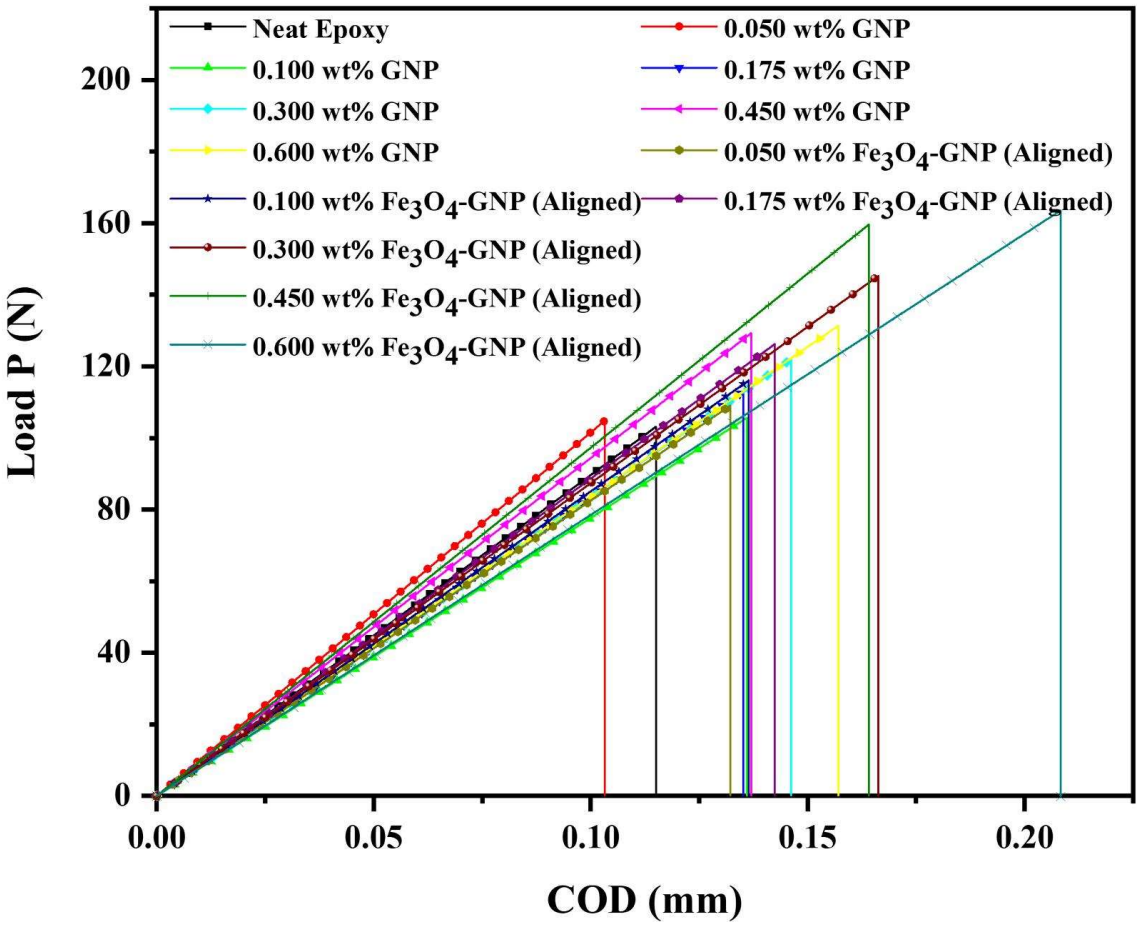

Fig. 5.14. Indicates the load and crack opening displacment (COD) behaviour of the nanocomposites under compact tension test at crosshead rates of 0.1 mm/min and ambient conditions (30 ^{0}C, humidity 50%).

5.4.3.1. Maximum CT load

Fig. 5.15 shows the maximum load before fracture of CT specimens loaded with nanoparticles. Adding GNP and aligned Fe_3O_4-GNP nanoparticles increased the maximum load for nanocomposites at different wt% levels, following a consistent trend of increase. Aligned Fe_3O_4-GNP nanoparticles had a superior effect to GNP, suggesting they can effectively enhance the mechanical properties of nanocomposites. The increased fracture load is directly related to fracture toughness, which is crucial for material durability and reliability.

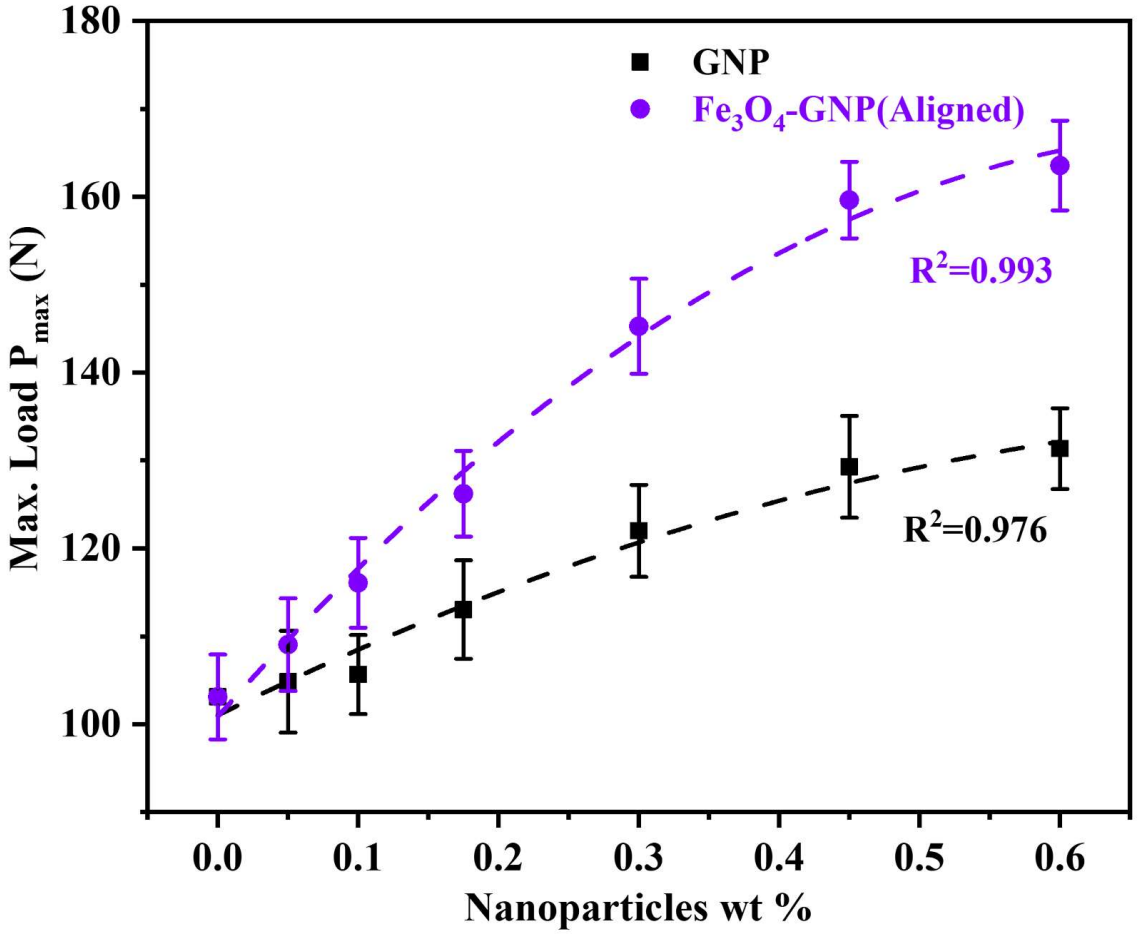

Fig. 5.15. Shows the maximum load sustained by the nanocomposite under compact tension test with different nanoparticle weight percentages. The error bar represents the Standard Deviation of data. The dotted line indicates that a polynomial adequately fits the data, while R^2 determined the quality of fit.

5.4.3.2. Stress intensity factor

Fig. 5.16 shows the critical stress intensity factor (Kcr) for different weight percentages of GNP and aligned Fe_3O_4-GNP nanoparticles. Kcr measures the energy required to initiate or resist unstable crack propagation. The nanocomposite's fracture toughness (K_{IC}) with both types of nanoparticles increases as the loading wt% increases. However, only the aligned Fe_3O_4-GNP nanocomposites show a significant increase in fracture toughness. The K_{IC} value for pure epoxy is 0.94 ± 0.020 MPa $m^{1/2}$, while the maximum K_{IC} values for GNP and aligned Fe_3O_4-GNP nanocomposites are 1.2 ± 0.04 MPa $m^{1/2}$ and 1.49 ± 0.03 MPa $m^{1/2}$, respectively, at 0.600 wt% for both loadings. These results indicate a significant increase in fracture toughness of 27.39% and 58.64% for the respective aligned Fe_3O_4-GNP and GNP loadings. Moreover, the nanocomposite with aligned Fe_3O_4-GNP loading has higher stiffness due to the alignment of the nanoparticles.

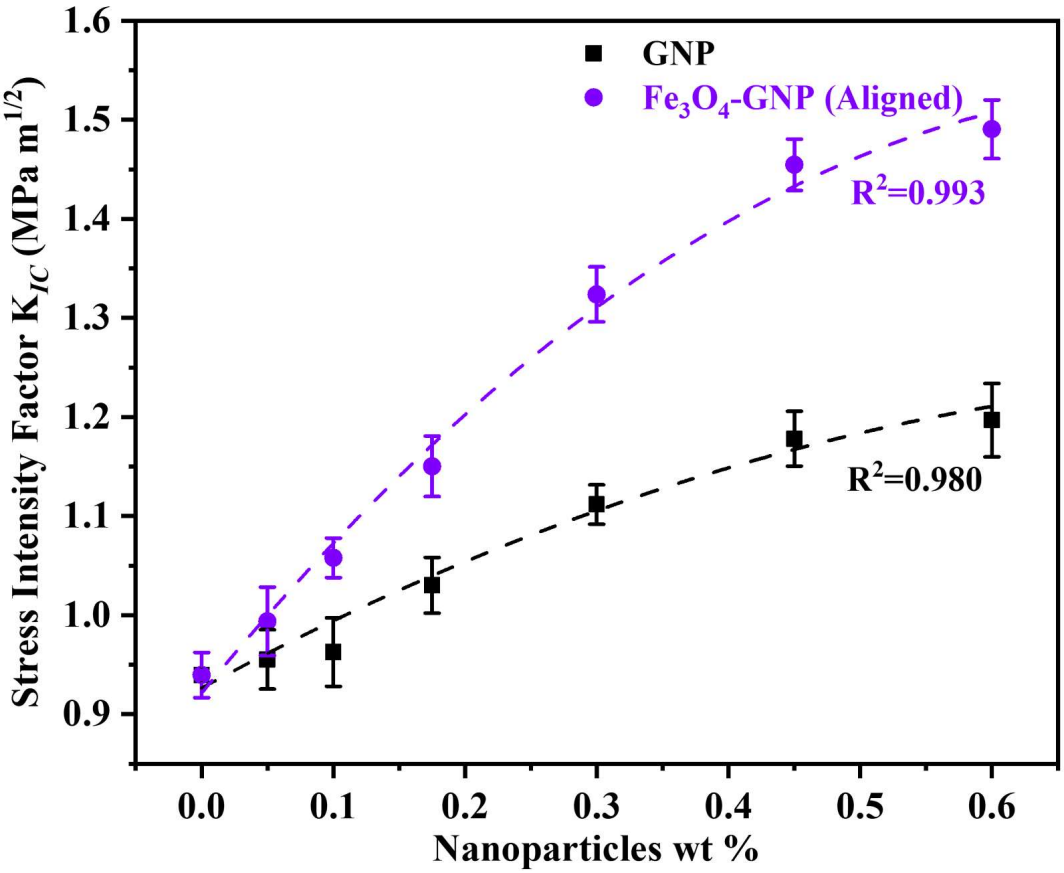

Fig. 5.16. Shows the Stress intensity factor of the nanocomposite with different nanoparticle weight percentages. The error bar represents the Standard Deviation of data. The dotted line indicates that a polynomial adequately fits the data, while R^2 determined the quality of fit.

5.4.3.3. Strain energy release rate

Fig. 5.17 shows that the critical strain energy release rate (G_{IC}) for pristine epoxy and its nanocomposites incorporating GNP and aligned Fe_3O_4-GNP nanoparticles consistently increases as the weight percentage of both GNP and aligned Fe_3O_4-GNP nanoparticles rises, peaking at 0.600 wt%. The orientation of Fe_3O_4-GNP particles significantly impacts the enhancement of G_{IC}. At 0.600 wt%, the G_{IC} of neat epoxy improved from 209.12 ± 16.780 to 301.39 ± 27.22 J/m^2 for GNP-reinforced nanoparticles (a 44.12% increase) and from 209.12 ± 16.780 to 419.92 ± 21.76 J/m^2 for aligned Fe_3O_4-GNP-reinforced nanoparticles (a 100.8% improvement) [2]. These findings suggest that incorporating GNP and aligned Fe_3O_4-GNP nanoparticles into epoxy can significantly enhance its critical strain energy release rate, with

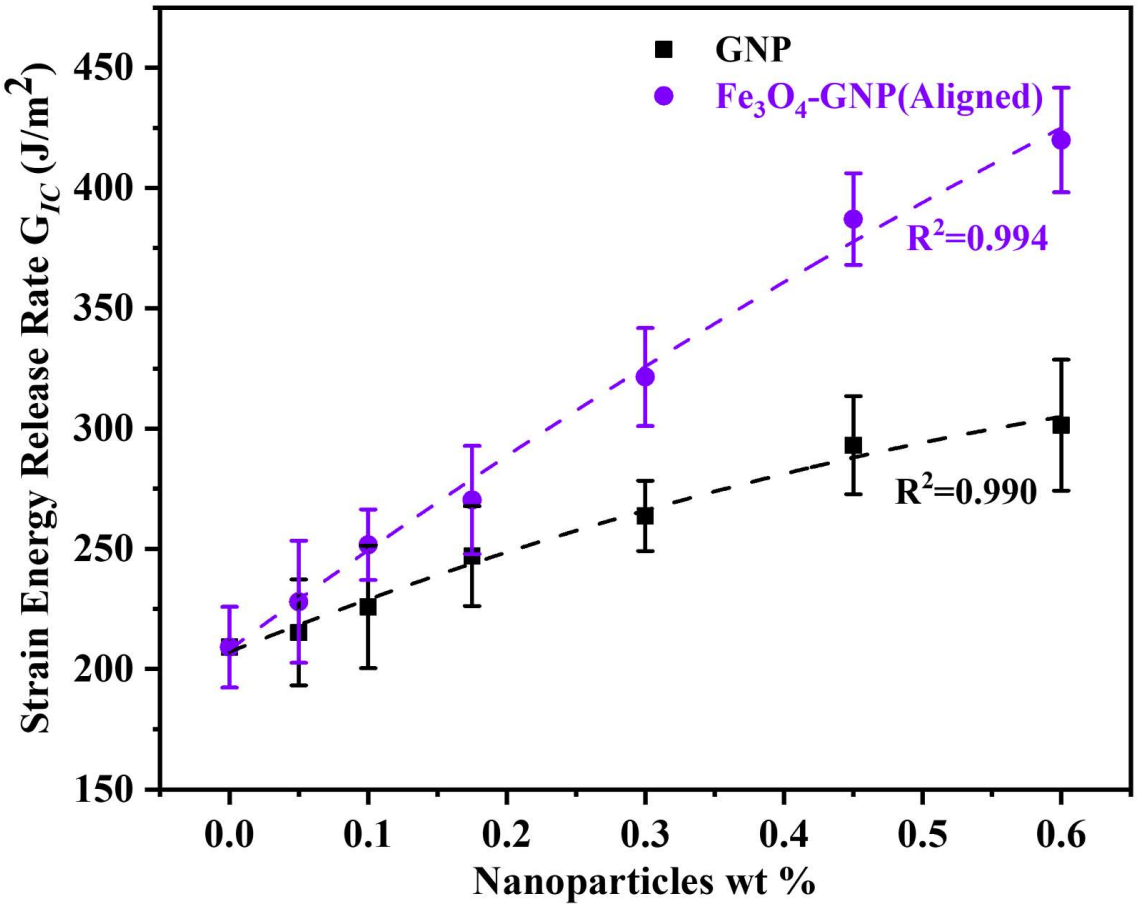

Fig. 5.17. Shows the Strain energy release rate of the nanocomposite with different nanoparticle weight percentages. The error bar represents the Standard Deviation of data.

the most substantial improvement observed in aligned Fe_3O_4-GNP-reinforced nanoparticles at 0.600 wt%.

5.4.3.4. Critical Crack Tip opening displacement

In a study examining the effect of GNP and aligned Fe_3O_4-GNP nanoparticles on crack displacement, we utilised Eq. (5.5) and COD to measure the critical $CTOD_c$ values. The results showed that both types of nanoparticles increased $CTOD_c$, leading to crack propagation and an increased displacement of the crack flanks (**Fig. 5.18**). The study also found that nanocomposites with a high concentration of nanoparticles exhibited stick/slip crack propagation due to crack tip blunting from localised shear yielding[207]. The critical stress intensity factor K_{IC} necessary to initiate a blunt crack was observed to be greater than that required to initiate a sharp crack[202]. The relationship between the ratio of critical stress intensity factors (K_{IC}) and the corresponding crack tip radii ratio was established, which is approximately equivalent to $CTOD_c$. The study assumed that the initial cracks in both epoxy and nanocomposites were sharp, and the effect of blunting in nanocomposites was approximated by comparing the fracture toughness values between nanocomposites and epoxy. The results from **Fig. 5.18** showed that the $CTOD_c$ of the nanocomposites increased with the loading weight percentage of both nanoparticles, with the effect of aligned Fe_3O_4-GNP being superior to that of GNP. Furthermore, the blunting of the crack increased with the nanoparticles, with aligned Fe_3O_4-GNP playing a critical role in improving the K_{IC} due to the blunting phenomena (**Fig. 5.19**).

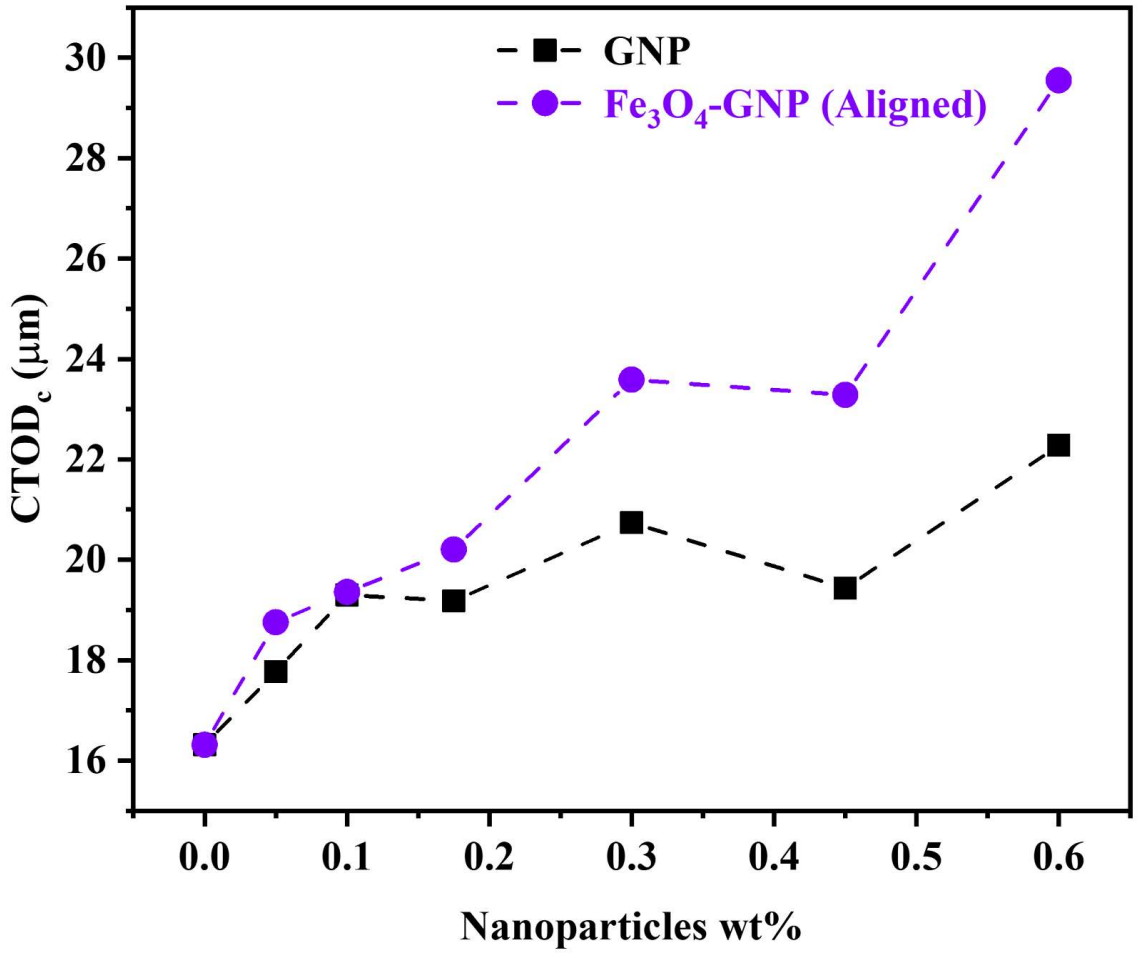

Fig. 5.18. Displays the crack tip opening displacement of nanocomposite with different nanoparticle weight percentages during the fracture .

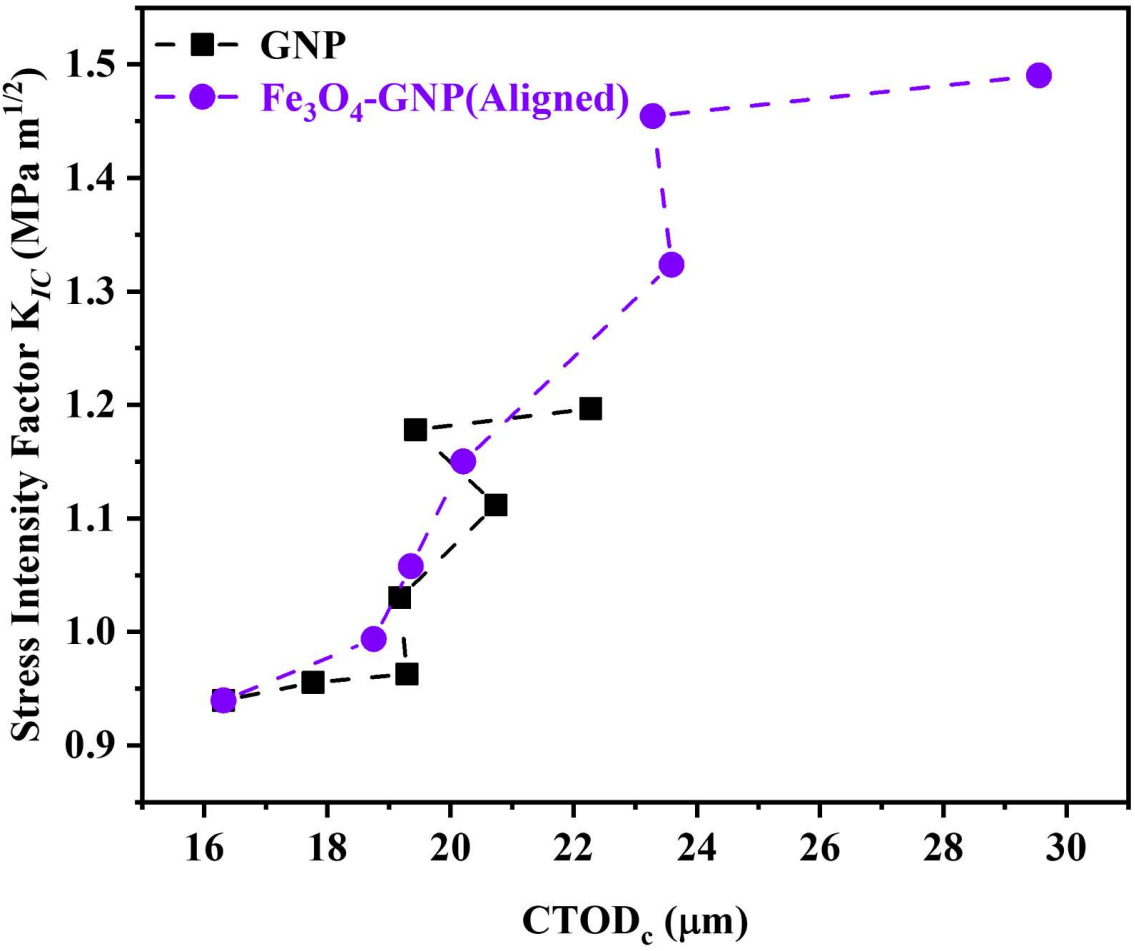

Fig. 5.19. Displays the stress intensity factor of the nanocomposite at differents Crack Tip opening displacement during the fracture.

5.4.4. Fracture surface analysis

5.4.4.1. Stereo zoom optical microscopy

The ability of a material to resist crack propagation is critical in preventing material failure, with the whitening zone on fractured surfaces indicating resistance to crack propagation via brittle fracture. This has helped identify fracture mechanisms in polymer nanocomposites, with optical microscopy images showing crack initiation and wrinkles in neat epoxy, GNP, and aligned Fe_3O_4-GNP nanoparticles reinforced nanocomposites (**Fig. 5.20**). Fractured surface morphology strongly correlates with evaluated critical stress intensity values, influenced by nanoparticle type, weight percentage, and alignment.

Compared to neat epoxy, low concentrations of GNP and aligned Fe_3O_4-GNP have presented a steeper fractured surface with more wrinkles. Surface morphology for aligned FeO4-GNP nanoparticles has shown more wrinkles than GNP 0.300Wt%, which has correlated with more crack resistance for the aligned Fe_3O_4-GNP compared to GNP. The fractured surface having 0.600wt% of the nanocomposites, has shown even more wrinkles (**Fig. 5.20**). The wrinkles at different spots have represented different surface morphologies, with those at the notch representing the crack initiation and those after representing the growth of the crack as rivers stream, which appear as whitening zone-like surfaces. A careful examination of the fracture surface reveals the presence of numerous tortuous and fine river-like structures, characterised by hackles and ribbons, at the centre of the fracture surface. The depth of the river-like wrinkles has shown different textures for the loadings of the nanoparticles and alignment. At the end of fractured surfaces, the river-like texture seems to vanish as a stream at the riverbank, which is a sign of an impending fracture.

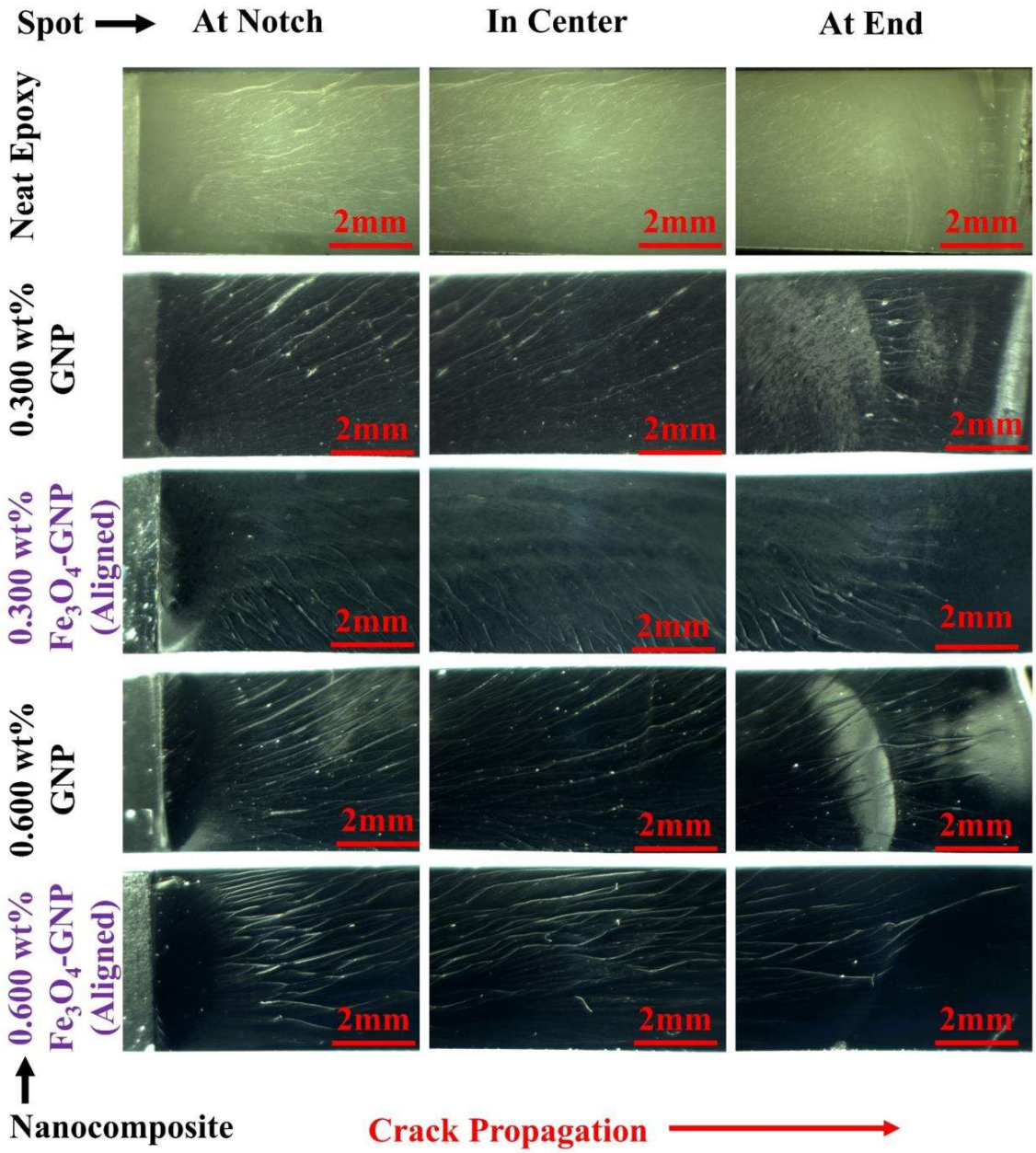

Fig. 5.20. Display stereo-zoom microscopic images of the fractured surfaces of the nanocomposites at three different spots for neat epoxy, 0.300wt%, and 0.600wt% of both GNP and Aligned Fe3O4-GNP nanoparticles.

5.4.4.2. Atomic force microscopy

The paragraph discusses the importance of assessing the roughness of multiple sections within the process zone to establish a correlation between the critical energy release rate of cracked nanocomposites and the fracture areas. The energy release rate is a key parameter in fracture

mechanics and refers to the energy required to propagate a crack per unit area. **Fig. 5.21** presents 3D AFM images of fracture surfaces and height profiles of GNP and aligned Fe_3O_4-GNP nanocomposites from an area of 10 x 10 μm to assess the impact of fracture surface profile on the toughening mechanism. The nanoparticle loading influences the amplitude functional surface roughness parameters for GNP and aligned Fe_3O_4-GNP nanocomposites, and these parameters increase with increasing wt% of nanoparticles in the epoxy matrix as well as more sensitive of alignments (Table 5.2).

Sa, the arithmetic average of 3D roughness, is commonly used for quality control of nano and micro roughness[208–210]. However, it does not provide information about the wavelength and is not sensitive to small changes in profile. When examining fractured surfaces of nanocomposites, it has been observed that the alignment of Fe_3O_4-GNP nanoparticles has a greater influence on roughness than nanoparticle loading (**Fig. 5.22)**. Aligned Fe_3O_4-GNP reinforced nanocomposites have significantly higher roughness values than those reinforced with GNP nanoparticles. For example, the Sa values of fracture surfaces of nanocomposites with GNP and aligned Fe_3O_4-GNP nanoparticles have been 213.48 nm and 455.68 nm, respectively. In comparison, the roughness of neat epoxy has only been measured as 9.27 nm (Table 5.2)**.** This indicates the effect of alignment on surface morphology, which is characteristic of the fracture behaviour of a ductile or toughened material.

In addition, the RMS parameter (S_q) denotes the standard deviation of surface heights and is more sensitive than the average height (Sa) in detecting deviations from the mean line. For neat epoxy, S_q is 7.30 nm, but for GNP and aligned Fe_3O_4-GNP nanoparticles reinforced nanocomposites, S_q values are 154.39 nm and 285.41 nm, respectively (Table 5.2). Moreover, alignment has more than doubled the S_q value of GNP nanoparticles nanocomposites.

Moreover, the parameter for maximum height, S_z, is determined as the difference in height between the average of the five highest peaks and the five lowest valleys along the surface

profile's assessment length. While S_z is a frequently used parameter, it is vulnerable to scratches, contamination, and measurement noise since it relies on peak values. The S_z values for neat epoxy, GNP, and aligned Fe_3O_4-GNP nanoparticle-reinforced nanocomposites are 90.55 nm, 1776.72 nm, and 2871.68 nm, respectively, providing evidence of the impact of alignment on fracture toughness (Table 5.2).

In addition, when high levels of aligned Fe_3O_4-GNP and nanofillers are present in nanocomposites, rigid nanoparticles cause propagating cracks to tilt or twist, resulting in increased peaks and valleys on fracture surfaces. Furthermore, crack deflection generates larger fracture surfaces than unaltered cracks, with higher surface variation observed for aligned Fe_3O_4-GNP and increased loading of GNP and aligned Fe_3O_4-GNP, as shown in Table 5.2.Matrix plastic deformation causes surface roughness and dissipates fracture energy, resulting in significant energy dissipation [211,212].

Table 5.2 shows the volume parameter, which integrates the surface height over 10 x10 μm, and the variation in roughness computed as the integral of the local gradient. The volume parameter reflects the roughness caused by nanoparticles, with values of 3.85 μm^3 for neat epoxy, 3.85 μm^3, 76.91 μm^3, and 121.39 μm^3 for Fe_3O_4-GNP. This indicates that aligned Fe_3O_4-GNP acts as an obstacle in crack propagation. Additionally, skewness (S_{sk}) measures the deviation from the symmetry of a fracture surface about the mean line. A zero skewness indicates a symmetrical height distribution. from Table 5.2, Positive S_{sk} values in the nanocomposite suggest high peaks on fractured surfaces (**Fig. 5.21**).

Furthermore, kurtosis (S_{ku}) measures distribution tailedness, where $S_{ku} < 3$ means thin tails and $S_{ku} > 3$ means heavy tails. Some nanocomposites' peak distributions are uneven, with S_{ku} values varying between less than 3 and greater than 3.Table 5.2 shows 9 of 13 nanocomposites have S_{ku} values less than 3, indicating even height distribution, with **Fig. 5.21** providing visual evidence. Lastly, waviness is a type of macro roughness that appears periodically on uneven

surfaces. **Fig. 5.23** shows how wavelength, frequency, and amplitude vary with nanoparticle loading in fractured surfaces of nanocomposites with GNP and aligned Fe_3O_4-GNP nanoparticles. Alignment and higher nanoparticle loading play a critical role in fracture surface morphology.

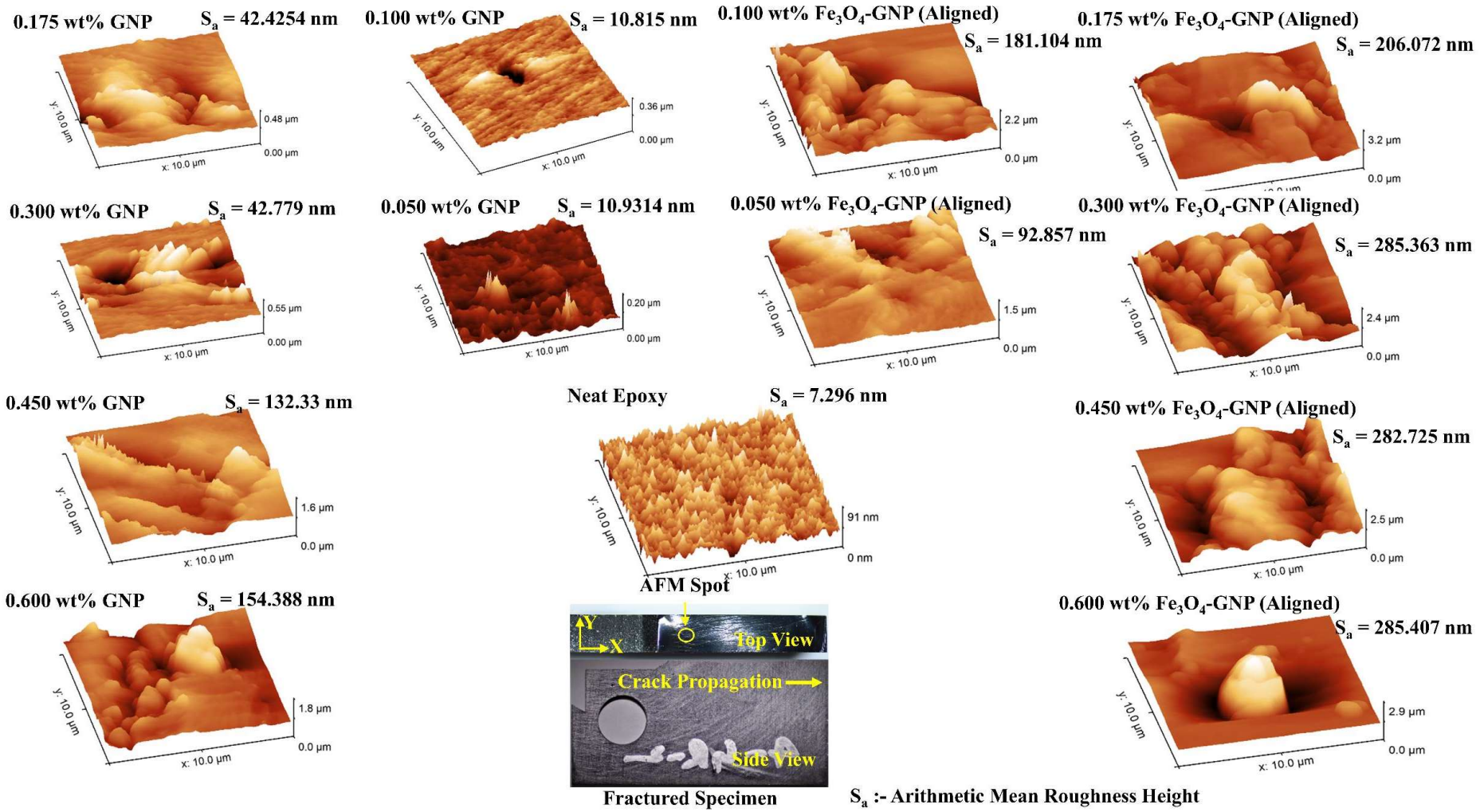

Fig. 5.21. Demonstrates the Atomic Force Microscope for 3D roughness parameters of the fractured surfaces of the nanocomposites.

Table 5.1. The sample designation and mechanical properties of nanocomposites with GNP and aligned Fe_3O_4-GNP nanoparticles.

Wt%	E (GPa)		σ_{yt} (MPa)		K_{IC} (MPa $m^{1/2}$)		G_{IC} (J/m^2)	
	GNP (↑)	**Fe_3O_4-GNP (↑)**	**GNP (↑↓)**	**Fe_3O_4-GNP (↑↓)**	**GNP (↑)**	**Fe_3O_4-GNP (↑)**	**GNP (↑)**	**Fe_3O_4-GNP (↑)**
Neat Epoxy	3.7 ±0.120 (0)	3.7 ±0.120 (0)	54.41 ±4.890 (0)	54.41 ±4.890 (0)	0.94 ±0.020 (0)	0.94 ±0.020 (0)	209.12 ±16.780 (0)	209.12 ±16.780 (0)
0.050	3.82 ±0.13 (3.27)	4.43 ±0.11 (19.55)	59.96 ±5.02 (10.22)	65.65 ±4.13 (20.67)	0.96 ±0.03 (1.69)	0.99 ±0.03 (5.78)	215.25 ±22.01 (2.93)	228.01 ±25.38 (9.03)
0.100	3.93 ±0.12 (6.08)	4.56 ±0.13 (23.12)	65.48 ±4.51 (20.35)	70.26 ±4.56 (29.15)	0.96 ±0.03 (2.47)	1.06 ±0.02 (12.59)	225.87 ±25.5 (8.01)	251.69 ±14.69 (20.36)
0.175	4.07 ±0.11 (9.98)	4.72 ±0.12 (27.56)	62.22 ±5.45 (14.35)	68.47 ±5.19 (25.85)	1.03 ±0.03 (9.65)	1.15 ±0.03 (22.43)	246.99 ±20.73 (18.11)	270.32 ±22.42 (29.26)
0.300	4.11 ±0.11 (11.04)	4.78 ±0.14 (29.14)	50.89 ±4.06 (-6.47)	70.12 ±4.09 (28.87)	1.11 ±0.02 (18.33)	1.32 ±0.03 (40.89)	263.71 ±14.64 (26.1)	321.45 ±20.35 (53.71)
0.450	4.16 ±0.13 (12.25)	4.8 ±0.15 (29.52)	48.41 ±4.53 (-11.02)	62.28 ±4.57 (14.47)	1.18 ±0.03 (25.39)	1.45 ±0.03 (54.82)	293.07 ±20.35 (40.14)	387.03 ±19.03 (85.07)
0.60	4.36 ±0.12 (17.73)	4.84 ±0.11 (30.73)	43.1 ±5.25 (-20.79)	50.92 ±4.5 (-6.4)	1.2 ±0.04 (27.39)	1.49 ±0.03 (58.64)	301.39 ±27.22 (44.12)	419.92 ±21.76 (100.8)

Note: - The ↑, ↓ denotes increments or decrements % values in the bracket, respectively.

Table 5.2: The sample designation and roughness parameters of fractured surfaces for nanocomposites with GNP and aligned Fe_3O_4-GNP nanoparticle

wt%	RMS Roughness, Sq, (nm)		Mean roughness, Sa, (nm)		Maximum height, Sz, (nm)		Area Variation (μm^2)		Volume (μm^3)		Skew (S_{sk})		Excess kurtosis (S_{ku})	
	GNP	**Fe_3O_4-GNP**	**GNP**	**Fe_3O_4-GNP**	**GNP**	**Fe_3O_4-GNP**	**GNP**	**Fe_3O_4-GNP**	**GNP**	**Fe_3O_4-GNP**	**GNP**	**Fe_3O_4-GNP**	**GNP**	**Fe_3O_4-GNP**
Neat Epoxy	9.27	9.27	7.30	7.30	90.55	90.55	11.03	11.03	3.85	3.85	0.15	0.15	0.55	0.55
0.050	15.32	139.05	10.93	92.86	195.88	1532.21	8.10	39.16	4.69	68.84	1.68	0.20	8.92	3.38
0.100	19.34	248.81	10.82	181.10	355.49	2174.91	11.32	74.41	28.29	103.24	-4.71	-0.09	49.41	1.09
0.175	58.54	313.52	42.43	206.07	475.15	3182.39	13.23	73.01	25.85	136.05	-0.09	0.71	1.34	5.04
0.300	66.44	351.37	42.78	285.36	546.95	2420.46	19.72	95.18	29.23	94.21	0.07	0.31	2.53	-0.36
0.450	176.70	362.63	132.33	282.73	1604.83	2465.61	47.53	66.72	82.96	109.68	-0.45	-0.01	1.47	-0.03
0.600	213.48	455.68	154.39	285.41	1776.72	2871.68	48.08	52.39	76.91	121.39	0.59	0.71	2.14	2.05

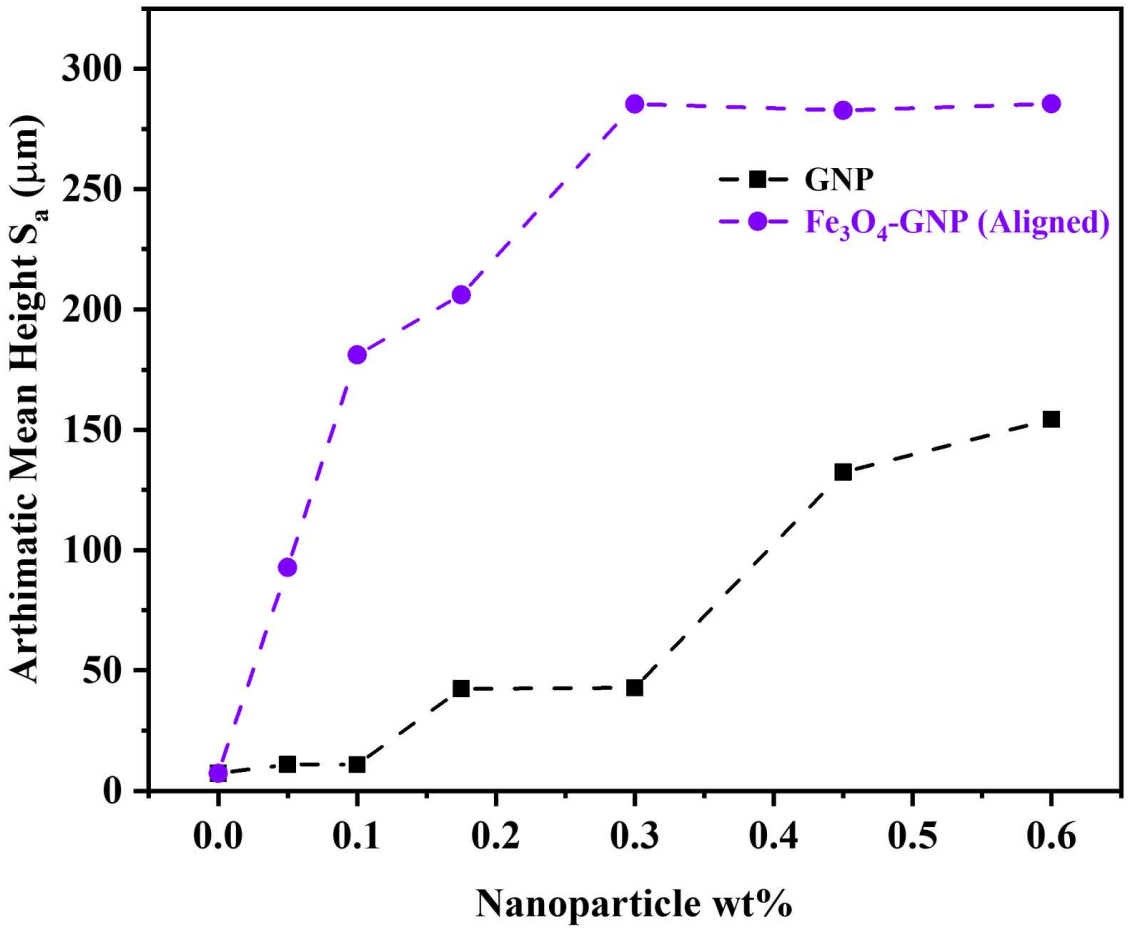

Fig. 5.22. Shows the roughness of the fracture surface of the nanocomposite with differents nanoparticles. The error bar represents the Standard Deviation of data.

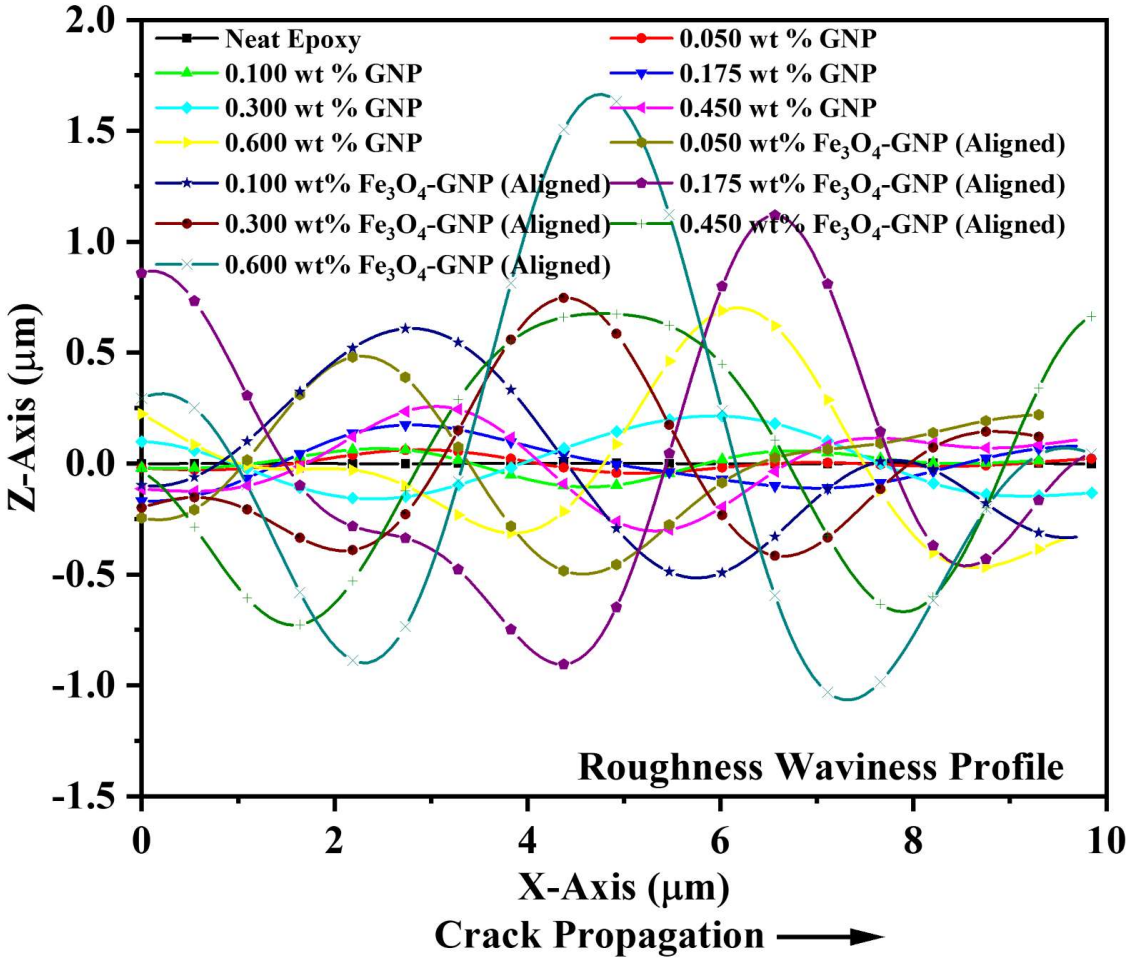

Fig. 5.23. Shows the roughness wavinessprofile of the fracture surface of the nanocomposite with differents nanoparticles.

5.5. Discussion

In the previous section (**5.2** and **5.4**), our discussion focused on the experimental setup, procedure, and individual test results, highlighting the influence of nanoparticle loading and the significant impact of the alignment of Fe_3O_4-GNP on the nanocomposite. However, an in-depth analysis of the underlying factors responsible for these outcomes and their implications on the nanocomposites' properties is yet to be presented. Ongoing discussions and investigations aim to gain a more comprehensive understanding of the situation. We will present the discussion in this section.

The reinforcement of nanoparticles in polymer matrices has been a challenging problem, as it depends on several interrelated factors, such as load transfer, stress concentration, and defect

distribution, which can either enhance or detract from the reinforcement effect. The tensile properties of nanoparticle-reinforced composites are primarily governed by the dominant mechanism of load transfer, which acts as a buffer against deformation and fracture. This mechanism will be discussed in more detail below, along with the relationship between the complex microscopic structure of the nanocomposites and the universal hydrodynamic reinforcement of nanoparticles and their fractal aggregates.

The mild improvement in tensile properties of GNP and aligned Fe_3O_4-GNP nanoparticles reinforced nanocomposites can be attributed to weak interfacial bonding between the nanoparticle sheets and the surrounding epoxy[213]. Load transfer from the epoxy to the nanoparticle sheets is not large enough to break the sheets under loading, resulting in sub-critical GNP-related failures that relieve overstress on the nanoparticles and reduce interfacial failures. The strain-softening at high strain is suggested to be due to sub-critical cracks resulting from GNP and aligned Fe_3O_4-GNP-related failure events. AFM images (**Fig. 5.21**) provided evidence of debonding of both GNP and aligned Fe_3O_4-GNP.

In addition, weak van der Waals forces exist between individual sheets of the nanoparticles, which can result in slipping between the sheets [214]. Finally, a recent study (4.3.6) observed that most of the nanoparticle sheets incorporated into the epoxy matrix exhibited noticeable curvature. Under tensile loading, these sheets required extension and rotation along the direction of the applied stress to optimise their contribution to the tensile modulus. However, the reinforcement effect of composites was limited due to the presence of wrinkling in both the GNP and aligned Fe_3O_4-GNP.

The presence of a soft interphase of epoxy has reduced the actual strain experienced by both the GNP and aligned Fe_3O_4-GNP, impacting the overall strain capacity of the composite material. The fine dispersion of GNP and aligned Fe_3O_4-GNP may have hindered the interphase's ability to evaluate plastic strain during tension, limiting the composite's

deformation capacity. However, Fe_3O_4 nanoparticles on GNP surfaces create micro-crazing, impeding crack propagation and improving tensile properties[215]. Fe_3O_4 also forms voids that limit the micro-damage spread, suggesting better mechanical interlocking and adhesion with the epoxy. The rough, wrinkled Fe_3O_4-GNP texture may have aided the improvement. Higher wt% of reinforcing nanoparticles may form agglomerates, resulting in less ductile interphases. Nevertheless, a higher concentration of aligned Fe_3O_4-GNP exhibited high ductility, providing evidence for a mechanism involving essential loading transfer through the tilting of the nano-reinforcement. Aligned nanoparticles played a critical role in improving mechanical properties, increasing stiffness but reducing the ductility and strength of nanocomposites.

The compressive properties of graphitic-based fillers, such as GNP and aligned Fe_3O_4-GNP, have demonstrated improvement with increasing nanoparticle loadings, as depicted in (**Fig. 5.11** and **Fig. 5.13**). The load transfer from the epoxy to nanoparticles has facilitated the increase in loading. Notably, aligned Fe_3O_4-GNP has played a critical role in load transfer, and its contribution has been more significant than that of GNP loading. During compression loading, the micro-crack has been suppressed, effectively preventing crack growth, and the resulting compressive strength has been due to the crushing of the epoxy. The significant improvement in compressive properties has been attributed to the load transfer and load-bearing capacity provided by the nanoparticles, which act as column-like structures during load carrying. Among the nanoparticles, aligned Fe_3O_4-GNP has played the most crucial role as a column-like structure, as shown in the results discussed in section **5.4.2**.

The crack tip in neat epoxy has been precisely characterised without detecting any damage mechanisms ahead of it, consistent with the behaviour of brittle-like polymers with low fracture toughness values (**Fig. 5.20**). However, adding GNP and aligned Fe_3O_4-GNP nanoparticles alters the fracture process at the main crack tip and creates a notably tortuous crack path in the nanocomposites. Aligned Fe_3O_4-GNP composites show more significant deviations than those

containing GNP alone, resulting in a significant development in the field. Stereo zoom optical images helped observe and analyse the deviation in the crack propagation route and growth behaviour at and ahead of the main crack tip.

According to the research findings presented in **Fig. 5.20** and **Fig. 5.21**, the inclusion of both GNP and aligned Fe_3O_4-GNP nanoparticles induces fracture and toughening processes in nanocomposites. This phenomenon is attributed to stress concentrations at interfaces between the epoxy and nanoparticles caused by a mismatch in Young's modulus and Poisson's ratio. The AFM imaging has revealed the presence of microcracks due to delamination and interfacial debonding. These observations suggest weaker bonding at the GNP and the epoxy-GNP interface, while a much stronger bonding was observed at the Fe_3O_4-GNP and the epoxy-Fe_3O_4-GNP interface. The formation of microcracks before the primary crack is recognised as an inherent toughening mechanism that enhances the fracture toughness of materials with low toughness, such as epoxy. However, microcracking is also a significant contributor to material failure.

The stereo zoom optical images in **Fig. 5.20** shows that isolated microcracks have merged to form a network of elongated cracks, which then joined the main crack front, contributing to intrinsic toughening and increased fracture toughness of the nanocomposites. **Fig. 5.21** shows that crack surfaces of nanocomposites with increased GNP and aligned Fe_3O_4-GNP have a higher surface roughness (as reported in Table 5.2) due to enhanced crack bifurcation and branching, leading to improved toughness of the epoxy nanocomposites. The alignment of Fe_3O_4-GNP in the epoxy nanocomposites increased the probability of the main crack encountering them, inducing more crack deflection and branching, resulting in a significant enhancement of the epoxy nanocomposites' toughening effect. Additional fracture toughening mechanisms were observed through AFM imaging, which will be further elaborated in subsequent sections.

The discussion regarding the toughening mechanisms in nanoparticle-reinforced epoxies has been ongoing for several years. It is generally accepted that debonding and cavitation must occur to activate more significant energy dissipation mechanisms, such as void expansion, matrix shear deformation, crack deflection, twisting, and bridging. All of these contribute to the overall fracture energy [216–220]. The ability of a material to resist fracture, particularly with respect to the propagation of cracks, is of paramount importance in engineering. The fracture behaviour of resins reinforced with nanoparticles is a multifaceted phenomenon and has been extensively studied in the literature, as evidenced by references such as [190,221].

When a crack front encounters nanoparticles, it has to propagate through the path between these particles, which is called crack pinning. This process can lead to a bow-shaped deformation, as observed in the waviness profiles (**Fig. 5.23**). Our investigation has shown that the nanoparticle reinforcements and the orientation of the nanoparticles influences the deformation of the crack front. In particular, the waviness profiles for aligned Fe_3O_4-GNP exhibit significantly more amplitude. GNP and Fe_3O_4-GNP are disk-shaped particles. Examination of the fracture surfaces of the samples and various roughness parameters, including S_q, S_a, S_z, variation, volume, S_{sk}, and S_{ku} (Table 5.2), has revealed that the highest resistance against crack propagation is achieved with aligned Fe_3O_4-GNP.

The S_{sk} and S_{ku} of AFM images (Table 5.2) show evidence of pulled-out GNP and aligned Fe_3O_4-GNP nanoparticles from one side of the fracture surface, indicating bridging of the crack faces under mode-I fracture. The jaggedly curved edges of both types of nanoparticles enhance the fracture toughness of the resulting nanocomposite by providing added resistance against pull-out forces via the mechanical lock phenomenon (**Fig. 5.21** and **Fig. 5.23**). Examination of the crack tip opening displacement (**Fig. 5.18**) reveals fracture and pull-out of nanoparticles, and both GNP and aligned Fe_3O_4-GNP initially bridge the crack over a crack-opening distance

of up to 22.29 μm and 29.55 μm, respectively, directly correlated to the fracture toughness and critical energy release rate (**Fig. 5.19).**

The presence of nanoparticles causes a shift in stress state from plane strain to plane stress conditions, inducing shear yielding in epoxy [7,222]. This change is attributed to voids, cavities, and debonding effects at the crack tip due to local constraints generated by the nanoparticles. Even though the specimen thickness is 4 mm, the nanoparticles act as local constraints, changing from two-dimensional to three-dimensional strains around the crack tip [223]. This leads to an increased plastic deformation zone near the crack front, allowing the specimen to tolerate more loads and exhibit a higher critical stress intensity factor [220]. The geometrical shapes and morphology of nanoparticles lead to an increasing trend of K_{IC} in nanocomposites, with the most effective enhancement achieved at 0.600wt% aligned Fe_3O_4-GNP loading. The crack-bridging mechanism enhances the fracture toughness of the epoxy resin [53].

5.6.Conclusions

The present study investigated the fabrication and mechanical properties characterisation of nanocomposites comprising GNP and aligned Fe_3O_4-GNP, which serve as nanoparticle reinforcements. Significant emphasis was placed on achieving an adequate dispersion of GNP and F3O4-GNP, as well as aligning Fe_3O_4-GNP in an epoxy matrix, to enhance the comparative investigation of the mechanical properties of the nanocomposite through the dual nanoparticle reinforcement. Aligned Fe_3O_4-GNP nanoparticles led to a more substantial improvement in mechanical properties, fracture toughness, crack propagation resistance and encounter more toughening mechanisms than GNP reinforcement alone, suggesting the potential of aligned Fe_3O_4-GNP reinforced nanocomposites as superior materials for engineering applications.